NMDAR MEDIATED CALCIUM TRANSIENTS ELICITED BY GLUTAMATE CO-RELEASE AT DEVELOPING INHIBITORY SYNAPSES IN THE AUDITORY BRAINSTEM

by

Abigail Susan Kalmbach

B.S.Eng. Princeton University, 2000

Submitted to the Graduate Faculty of

The School of Medicine in partial fulfillment

of the requirements for the degree of

Masters of Science

University of Pittsburgh

2008

UNIVERSITY OF PITTSBURGH

SCHOOL OF MEDICINE

This thesis was presented

By

Abigail Susan Kalmbach

It was defended on

July 26, 2008

and approved by

Daniel J. Simons, Professor, Department of Neurobiology

Guo-Qiang Bi, Associate Professor, Department of Neurobiology

Thesis Advisor: Karl Kandler, Associate Professor, Department of Otolaryngology

NMDAR MEDIATED CALCIUM TRANSIENTS ELICITED BY GLUTAMATE CO-RELEASE AT DEVELOPING INHIBITORY SYNAPSES IN THE AUDITORY BRAINSTEM

Abigail Kalmbach, M.S.

University of Pittsburgh, 2008

Before hearing onset, synapses in the inhibitory pathway from the medial nucleus of the trapezoid body (MNTB) to the lateral superior olive (LSO) not only release GABA and glycine, but also glutamate. This transient glutamate release from nominally inhibitory synapses coincides with the period in which the MNTB-LSO pathway is tonotopically refined. I hypothesized that by releasing glutamate, developing MNTB-LSO synapses can elicit NMDA receptor (NMDAR) mediated calcium influx, which has been shown to underlie the refinement of excitatory topographic maps.

To test my hypothesis, I designed and built a 2-photon microscopy system to perform two complementary series of calcium (Ca^{2+}) imaging experiments. The objective of the first series of experiments was to investigate the potential of developing MNTB-LSO synapses to elicit NMDAR-mediated Ca^{2+} responses. Experiments were performed under conditions that maximized the ability for GABA/glycinergic conductances to aid in the relief of magnesium (Mg^{2+}) block at NMDARs. Electrical stimulation of the MNTB-LSO pathway consistently elicited local Ca^{2+} transients in LSO dendrites that were significantly reduced by NMDAR antagonists. Despite their significant contribution to MNTB-elicited dendritic Ca^{2+} responses, NMDARs did not contribute to somatically recorded electrical responses.

In the second series of experiments, I investigated the ability for MNTB-LSO synapses to activate NMDAR-mediated Ca^{2+} transients using only imaging techniques.

Here we found that MNTB-LSO inputs by themselves could not elicit somatic NMDAR-mediated Ca^{2+} responses when GABA/glycinergic conductances were present with extracellular Mg^{+}, despite having the potential to elicit these Ca^{2+} responses. These results suggest that GABA/glycinergic conductances shunt the somatically-recorded Ca^{2+} response. They raise the question of whether MNTB-LSO inputs can elicit local dendritic NMDAR-mediated Ca^{2+} responses independently from other LSO inputs.

Together, these experiments demonstrate the ability of developing MNTB-LSO inputs to activate NMDAR Ca^{2+} signaling pathways during the time of topographic map refinement. Although this ability was only observed under conditions that altered or abolished GABA/glycinergic conductances or extracellular Mg^{2+}, this ability could endow developing inhibitory synapses with a novel and potentially powerful refinement mechanism to be activated under physiological conditions.

TABLE OF CONTENTS

LIST OF FIGURES

ACKNOWLEDGMENTS

The unfaltering support of my family and friends gave me the strength and confidence to pursue a graduate degree. My parents and three brothers never let me doubt for a minute that I could succeed at whatever I put my mind to and was passionate about. They also helped me to realize that my decision to leave the Kandler lab with a masters and not doctoral degree was a mark of bravery. Thank you for giving me the confidence to follow my dreams. This work is dedicated to my parents, brothers and grandparents (living and deceased).

My friends provided a lifeline for me throughout my years in Pittsburgh. Jason Castro has been a pillar of support and a scientist to emulate. Lesley Colgan has been a steadfast friend and soccer teammate throughout these years. Rick Gerkin and David Nauen were founts of experimental tips and fun science discussions. Krishnan Padmanabhan and Vikrant Kapoor were loyal bbq-ers and friends. Tamara Berdyyeva was a confidant and an inspiration of dedication. And Chris Gaiteri was a great soccer buddy and I am grateful for his comments on this document. I also extend special word of gratitude to friends not noted by name here but remembered in my heart.

The large neuroscience community in Pittsburgh drew me to the city and welcomed me into the field. The Center for the Neural Basis of Cognition (CNBC) provided a social network for me when I first arrived and supported my pursuit of interdisciplinary research through coursework and an IGERT training grant. I am very appreciative of the time and guidance I received from Peter Strick, co-director of the CNBC. His sincere desire to do whatever necessary to see every student in the CNBC succeed is reflected in the strength of the program.

The Center for Neuroscience at the University of Pittsburgh (CNUP) and the Department of Neurobiology became my home-base once I joined the Kandler laboratory. Interactions with faculty and students gave me a breadth of understanding across the vast field of Neuroscience and stimulated my thinking regarding my own research.

I am grateful for everything that I learned from my adviser, Karl Kandler, particularly how to frame scientific questions, write grants, and present data. My doctoral thesis committee, consisting of Dan Simons, Guo-Qiang Bi, Justin Crowley and Alison Barth, gave me very helpful feedback and guidance on my research project. I am particularly appreciative of the sage advice that Dan Simons gave me as chair of my committee and co-chair of the CNUP. I would also like to thank Jon Rubin for advising me on my IGERT project and supporting me throughout.

The work presented in this thesis was funded by an NRSA pre-doctoral grant.

I. INTRODUCTION

Sensory information, gathered at the periphery, propagates through cascades of nuclei that filter and process the sensory signals. The accuracy and efficiency of this signal transmission is posited to be dependent on the preservation and the precision of the topographic mapping of the sensory input across successive nuclei. Molecular guidance cues initiate a coarse map characterized by abundant synapses from many different projection neurons resulting in very large and overlapping receptive fields (McLaughlin and O'Leary 2005). Activity-dependent processes then sculpt and refine this immature map to create a precise topological map for accurate signal transmission (Katz and Shatz 1996). The objective of the present study is to garner more insight into the mechanisms underlying this refinement process as it pertains to inhibitory topographic maps through the investigation of a first-order binaural sound localization circuit in the auditory brainstem.

The azimuth position of high frequency sound is initially calculated by principal neurons in the lateral superior olive (LSO) through the integration of tonotopically aligned excitatory and inhibitory synaptic inputs (Boudreau and Tsuchitani 1968). The excitatory, glutamatergic inputs to the LSO project from the ipsilateral cochlear nucleus (CN), while the inhibitory, glycinergic inputs project from the medial nucleus of the trapezoid body (MNTB), which receives excitatory inputs from the contralateral CN (Boudreau and Tsuchitani 1968; Cant and Casseday 1986).

Investigations of the MNTB-LSO pathway have found substantial refinement preceding hearing onset that is manifested in the functional elimination of most MNTB-LSO inputs and the strengthening of the remaining inputs (Kim and Kandler 2003). Concurrent with this period of refinement, the functional characteristics of the MNTB-LSO synapses undergo developmental changes including the polarity of

GABA/glycinergic transmission, which switches from depolarizing to hyperpolarizing (Kandler and Friauf 1995; Ehrlich et al. 1999; Kullmann and Kandler 2001). Additionally, and of particular interest to this study, the composition of neurotransmitters released at MNTB-LSO synapses transiently includes both the traditional inhibitory neurotransmitters, glycine and GABA (Kotak et al. 1998; Nabekura et al. 2004), as well as the canonical excitatory neurotransmitter, glutamate (Gillespie et al. 2005).

Numerous studies have demonstrated the importance of activating of calcium (Ca^{2+}) signaling pathways for induction of plasticity at inhibitory synapses (Stelzer et al. 1987; Grunze et al. 1996; McLean et al. 1996; Morishita and Sastry 1996; Wang and Stelzer 1996; Kotak and Sanes 2000; Ouardouz and Sastry 2000; Cavazzini et al. 2005; Marsden et al. 2007; Nugent et al. 2007). Work from our laboratory has shown the ability of MNTB inputs to elicit Ca^{2+} responses via voltage gated Ca^{2+} channels (VGCCs) during the developmental period when GABA/glycinergic conductances are depolarizing (Kullmann et al. 2002). In addition to this means of Ca^{2+}entry, the co-release of glutamate could endow developing MNTB-LSO synapses with the ability to access glutamate-mediated, local Ca^{2+} signaling pathways, namely via NMDA receptors (NMDARs). Since the co-release of glutamate and activation of NMDARs extends beyond the developmental period when GABA/glycinergic conductances are depolarizing but coincides with the period of tonotopic refinement (Kullmann and Kandler 2001; Kim and Kandler 2003; Gillespie et al. 2005), this latter means of eliciting Ca^{2+} entry could be an essential component in the refinement of the MNTB-LSO pathway. In support of this, NMDAR activation has been demonstrated to be instrumental in synaptic refinement at excitatory synapses (Cline et al. 1987; Cline and Constantine-Paton 1990) and in synaptic plasticity at excitatory and inhibitory synapses (see reviews (Malenka and Bear 2004; Nugent and Kauer 2008)).

Accurately distinguishing between superfluous synapses, which should be eliminated versus those pertinent synapses, which should be strengthened, is a fundamental process that underlies refinement. This is likely achieved by compartmentalizing and isolating biochemical signaling cascades initiated at active synapses. In many neurons, dendritic spines perform this function (see rev. (Yuste et al. 2000; Nimchinsky et al. 2002)). In cortical interneurons and cerbellar stellate cells which

have aspiny dendrites, however, compartmentalization is achieved with extrusion pumps with fast kinetics (Goldberg et al. 2003) and calcium binding proteins (Soler-Llavina and Sabatini 2006), respectively. A recent study from our laboratory demonstrated that Ca^{2+} responses at MNTB synapses onto aspiny LSO dendrites are also compartmentalized (Kullmann and Kandler 2008) but the mechanisms underlying this compartmentalization have yet to be determined.

In this study, we investigate several aspects of glutamate release on Ca^{2+} entry. We show the potential of MNTB-LSO synapses to elicit Ca^{2+} influx through NMDARs under depolarizing GABA/glycine conditions. We then explore experimental conditions under which NMDARs can be activated when the intracellular chloride (Cl^-) level is kept intact. Together, these experiments demonstrate the ability of developing inhibitory synapses to elicit localized, NMDAR mediated Ca^{2+} transients but this ability is apparently limited to conditions that circumvent the shunting induced by GABA/glycinergic conductances.

II. METHODS

A. Slice preparation

Experiments were performed in accordance with NIH guidelines and approved by IACUC at the University of Pittsburgh. Brainstem slices were prepared from mice (129S6/SvEv) postnatal 1-8 days (P1-8). Animals were anesthetized by Isofurane and decapitated. The brain was removed and submerged in artificial cerebrospinal fluid (ACSF; composition in mM: NaCl 124, $NaHCO_3$ 26, glucose 10, KCl 5, KH_2PO_4 1.25, $MgSO_4$ 1.3, $CaCl_2$ 2, and for slicing kynurenic acid 1; pH 7.3 when aerated with 95%O_2/5%CO_2). Coronal slices (250-300μm) were cut with a vibratome (Leica VT1000S) and slices containing the MNTB and LSO were allowed to recover for at least 1 hr in an interface chamber at room temperature.

B. Electrophysiological recording

Slices were continuously perfused with aerated ACSF (~3ml/min; composition as above and, for most experiments, with 100μM Trolox to protect against phototoxicity). Whole-cell patch clamp recordings were obtained from principal LSO neurons, visualized with an infrared optical gradient system (Luigs and Neumann, Germany). The pipette solution consisted of (in mM): K-gluconate 60, KCl 60, Na_2-phoshocreatine 10, HEPES 10, GTP-Na_2 0.3, ATP-Mg 4, the Ca^{2+} indicator, Oregon Green Bapta 0.1 (K_d=170nM),

and the sodium channel antagonist, QX314 5. The Cl^- reversal potential (E_{revCl-}) calculated from the Nernst equations was -20mV.

After gaining whole-cell access in voltage clamp, the cell was held in current clamp configuration and the indicator was allowed to diffuse into the cell for 20 minutes. Membrane potential changes to hyperpolarizing current steps (200ms, -10pA) followed by a single synaptic stimulus were monitored every 10-20 sec to measure stability of recording and synaptic input. The MNTB-LSO pathway was stimulated just lateral to the ipsilateral MNTB with a unipolar glass electrode (2-4MΩ input resistance).

C. Calcium imaging

2-photon imaging was performed with a Ti:Sapphire laser (Chameleon XR; Coherent) coupled to a custom-modified Olympus Fluoview 300 scanning system and upright microscope (BX50WI, Olympus), as described by other groups (Nikolenko et al. 2003; Yasuda et al. 2004). Non-descanned fluorescent emissions were collected with a photomultiplier tube (R6095; Hamamatsu) positioned at the epifluorescence port. FluoView software (Olympus) controlled the scanhead, triggered electrophysiological data acquisition and collected the imaging data (See Appendix for description of 2-photon imaging system). The spatial resolution of our imaging system was ~0.5 μm.

For dendritic Ca^{2+} imaging experiments (Fig 1-4), images were acquired as one-pixel-wide linescans at 100-200Hz (Fig 3d). The linescans were positioned along the dendritic axis (Fig 3a,b). The duration of each trial was 1.4 seconds with the stimulus (3-5 stimuli at 10Hz) onset at 0.2 sec. To control for slight displacements of the dendritic segment and to ensure that the same region of dendrite was imaged throughout the experiment, linescan images were visually compared with previous images for similar peaks and troughs. If necessary, line placement was adjusted for small lateral or vertical shifts in the image plane that sometimes occurred during the experiment. For analysis, images were aligned according to the peak of the cross correlograms between spatial profiles of the resting fluorescence from the first trial and each subsequent trial. The

spatial profile of the resting fluorescence was calculated along the spatial extent of the linescan from the average fluorescence intensity during the imaging period before stimulus onset. Data were only analyzed from cells in which the major peaks and troughs of the resting fluorescence overlapped following alignment (fig 1c) and the electrical recordings were stable through the control and drug conditions.

For somatic Ca^{2+} imaging experiments (Fig 5-7), brainstem slices were bulk-labeled with the Ca^{2+} indicator, Fura-2AM (100μM for 3min; 10μM for 60min; at 32°C), as described previously (Ene et al. 2003). Non-ratiometric imaging of Fura-2 was performed by exciting the dye at 810nm and recording the fluorescence emissions of Fura-2 unbound to Ca^{2+} (equivalent to measurements made with 380nm excitation). Ca^{2+} responses were thus recorded as a decrease in fluorescence. For analysis, data are plotted as $-(\Delta F/F)$ such that an increase in $[Ca^{2+}]_i$ is plotted as a positive value. MNTB stimulation patterns of 10 stimuli at 20Hz were used to maximize the elicited Ca responses. Data were collected in frame-scan mode with an acquisition rate of 2Hz and resolution of 512x224 pixels. Five trials were performed for each experimental condition.

D. Chemicals

The effects of the following pharmacological reagents on MNTB-evoked responses were investigated: DL-2-amino-5-phosphonovaleric acid (APV; 100μM), 6-cyano-7-nitroquinoxaline-2,3-dione (CNQX; 10μM, suspended in DMSO), Strychnine (Stry; 1μM), Bicuculline (Bic; 10μM), and SR95531 (SR; 10μM) (all chemicals from Sigma except SR which is from Tocris). 1000:1 Stock solutions of these compounds were stored at -20°C until used.

E. Analysis

For dendritic imaging experiments, linescan images were aligned (as described above), smoothed (3 pixel box filter), and analyzed with IgorPro (scripts modified from Dr. N. Urban; Wavemetrics, OR). The spatial (dendritic) axis of the linescans was divided into overlapping 3μm windows and Ca^{2+} responses were calculated for each window as done for framescan images. The reported Ca^{2+} response for each neuron was taken from the window containing the largest Ca^{2+} response during control conditions and/or the window spanning the dendritic region that was most stable throughout all recording conditions. The soma-dendritic distance of the Ca^{2+} response was measured from compressed z-stack images.

For somatic imaging experiments, framescan images were median-filtered (3x3 kernel), movement-corrected with TillVision (T.I.L.L. Photonics, Germany) and exported for further analysis with scripts custom-written in MATLAB (MathWorks, Ma). Background-subtracted fluorescence values were converted into changes in fluorescence relative to baseline ($\Delta F/F$). Successful trials, defined as those with increases in $\Delta F/F$ greater than 2 standard deviations of baseline, were averaged together within each imaging condition for each region of interest. Only cells with successful trials in the Mg-free condition were included for analysis.

III. RESULTS

A. NMDAR-mediated Ca^{2+} responses elicited at MNTB-LSO synapses

In addition to releasing GABA and glycine, MNTB axon terminals co-release glutamate that activates both AMPARs and NMDARs on postsynaptic LSO neurons, with the glutamatergic current influx predominantly mediated by NMDARs (Gillespie et al. 2005). Ca^{2+} influx via NMDARs is crucial for many forms of activity dependent refinement and plasticity both at glutamatergic and GABAergic synapses (see rev. (Gaiarsa et al. 2002; Malenka and Bear 2004; Ruthazer and Cline 2004)). This opens the possibility that NMDARs would significantly contribute to dendritic Ca^{2+} influx during the period of functional refinement in the MNTB-LSO circuit (Kim and Kandler 2003).

To investigate the potential of NMDARs to contribute to Ca^{2+} responses at MNTB-LSO synapses, we performed experiments under conditions that would maximize the ability for GABA/glycine activation to relieve the Mg^{2+} block at NMDARs. Our internal pipette solution induced a depolarizing $E_{Cl\text{-}rev}$ (-20mV) and blocked action potentials with QX314. Thus, we could elicit large MNTB-LSO PSPs while maintaining our ability to visualize subcellular dendritic Ca^{2+} domains.

MNTB-elicited Ca^{2+} responses were significantly mediated by NMDARs. Application of the specific NMDAR antagonist, DL-APV (100μM) reduced the dendritic Ca^{2+} response (Fig 1e, upper traces) without altering the amplitude of the first or decay time of the last somatically recorded PSP. In this example, however, it did reduce the amplitude of the last PSP (Fig 1e, lower traces). Across a population of 18 cells (from 18 animals, P4-7), we found that Ca^{2+} influx through NMDARs accounted for approximately one third the size of MNTB-elicited Ca^{2+} responses (34±9% reduction in

Ca^{2+} response following APV, n=18 cells, p<0.005, paired ttest, Fig 2a). These experiments likely underestimate the NMDAR contribution to the Ca^{2+} response that would occur under more physiological conditions, because under these experimental conditions, the depolarizing GABA/glycinergic conductances also contributed to the Ca^{2+} responses through the activation of VGCCs. However, this underestimation does not alter our primary finding that developing MNTB-LSO neurons have the potential to access NMDAR-mediated Ca^{2+} signaling pathways.

1. Phototoxicity control experiments: We performed a set of control experiments to determine whether the lack of response recovery after APV washout was due to phototoxicity. In these experiments, we used identical experimental parameters as in the normal drug experiments (including numbers of stimulations, trials, and times between trials), but did not apply APV after the baseline images were acquired. We found that the Ca^{2+} responses were stable throughout this experimental paradigm (mock-APV response normalized to control = 97.0±9.7; n=14 cells; p=0.45; normalized mock-wash response = 98.9±13.3%; n=6; p=0.9; Fig 2b). Furthermore, since partial washout was observed in some cells (3 of 7 cells held through wash, see Fig 1e for example), we doubt the lack of washout is biologically based. Rather, we believe washout was not observed because during the washout period in particular the baseline fluorescence intensity increased in many of the neurons. Thus, the washout could be eclipsed by a larger 'F' in the $\Delta F/F$ calculation. Indeed, when Ca^{2+} responses were reported as changes in fluorescence (ΔF) and not changes in fluorescence with respect to baseline fluorescence ($\Delta F/F$), the Ca^{2+} responses recovered in most cells (data not shown).

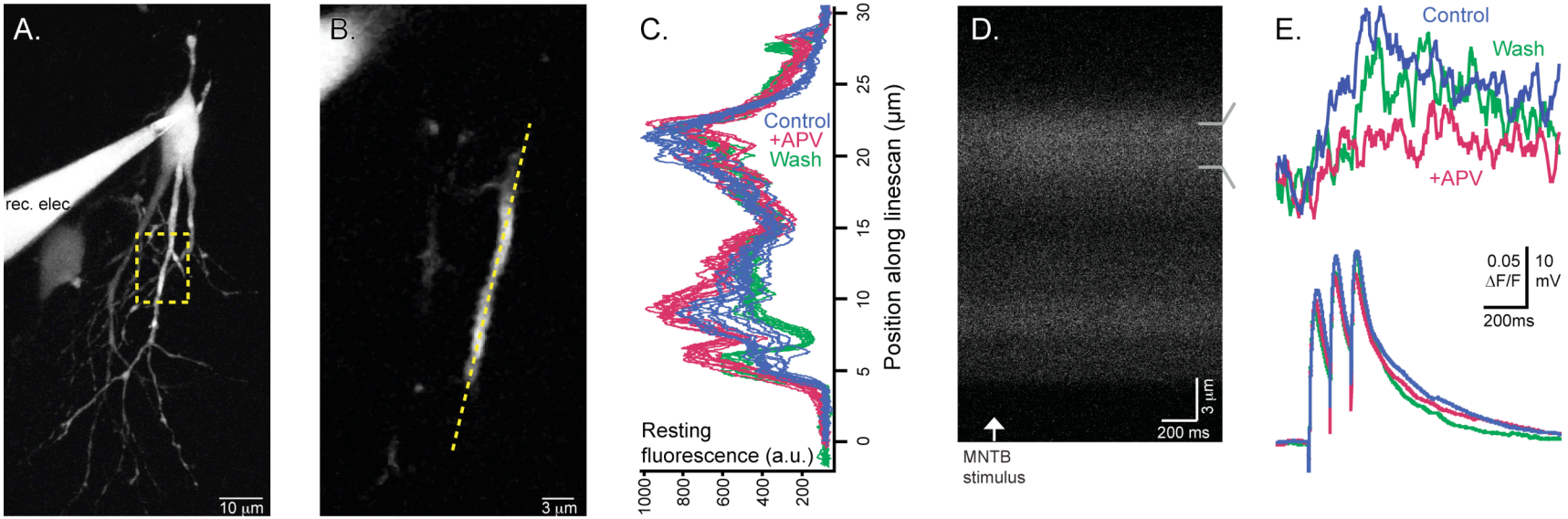

Figure 1: NMDARs significantly contribute to MNTB-elicited Ca^{2+} responses.
A. Compressed z-stack of recorded neuron (P5). Region of imaging is outlined.
B. Position of linescan (yellow dotted line) relative to dendrite within focal plane.
C. Alignment of baseline fluorescence intensity profile shows stability throughout experiment.
D. Linescan image of a single trial. Increase in fluorescence after MNTB stimulation indicates an increase in dendritic Ca^{2+} concentration.
E. *Upper traces:* MNTB-elicited Ca^{2+} response is significantly mediated by NMDARs, as demonstrated by a reduction in response following APV application.
Lower traces: Corresponding electrical responses. Traces are averages of 10 trials/condition.

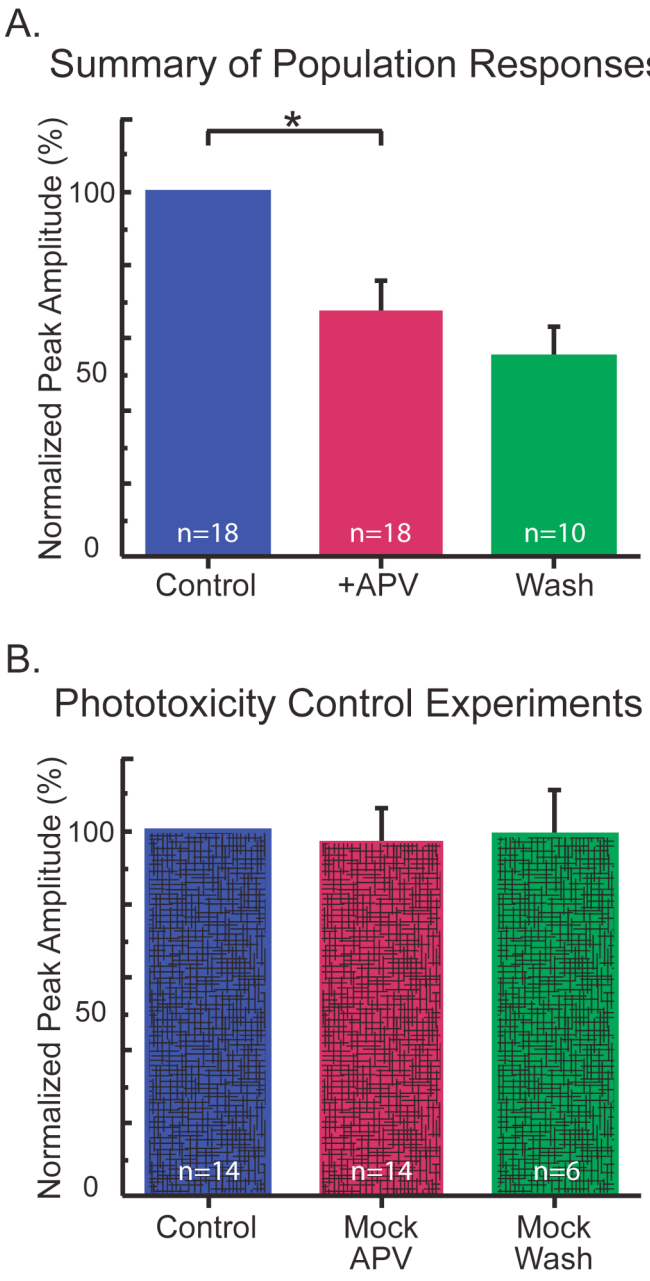

Figure 2: Summary of dendritic Ca^{2+} responses
A. MNTB-LSO elicited Ca^{2+} responses were significantly reduced following application of APV. Responses were not significantly different between APV and wash conditions.
B. Lack of washout is not due to phototoxicity: control experiments with identical recording conditions as above except no drug was applied following the first set of trials.

2. Contribution of NMDARs to Ca^{2+} responses are uncorrelated with dendritic location: Anatomical studies suggest that inhibitory inputs in mature LSO neurons primarily innervate the somatic and proximal dendritic region (Cant 1984; Helfert et al. 1992; Friauf et al. 1997). Were dendritic MNTB-LSO inputs eliminated and perisomatic inputs strengthened during development, we might expect to find a correlation between the soma-dendritic distance and the contribution of Ca^{2+} influx through NMDARs. This would be indicative of an association between the means of Ca^{2+} entry and the 'direction' of refinement and would be manifested in a dendritic gradient of NMDAR contributions to the Ca^{2+} response. For example, in the developing hippocampus, Ca^{2+} influx via NMDARs or VGCCs can elicit synaptic depression or potentiation, respectively (McLean et al. 1996). However, we observed no correlations between Ca^{2+} responses and dendritic locations with respect to either the peak Ca^{2+} responses in control and APV conditions (R^2=0.02, R^2=0.08. Fig 3a,b, respectively) or the percent change in Ca^{2+} response following APV application (R^2=0.11, Fig 3c). The lack of correlation indicates that the MNTB-LSO inputs along the first 50μm of the LSO principal dendrites form a uniform population of inputs with respect to Ca^{2+} response amplitude and means of Ca^{2+} entry. This suggests two possibilities: these inputs represent the set of inputs that are eventually either eliminated or strengthened; or these characteristics of Ca^{2+} entry are not indicative of the fate of these inputs.

It should be noted that in the two cells with responses located the farthest from the soma, application of APV resulted in an increase in the Ca^{2+} response. A larger sampling of responses at these distances is needed before any hypotheses or conclusions are drawn.

3. Somatically recorded PSPs are not affected by APV: Although NMDARs contribute to a large component of the Ca^{2+} responses across the population of neurons, they do not significantly contribute to the electrical responses at MNTB-LSO synapses, as recorded at the soma with high Cl^- (60mM) in the pipette. The amplitude of the first PSP was consistent across control, drug, and wash conditions (Control:

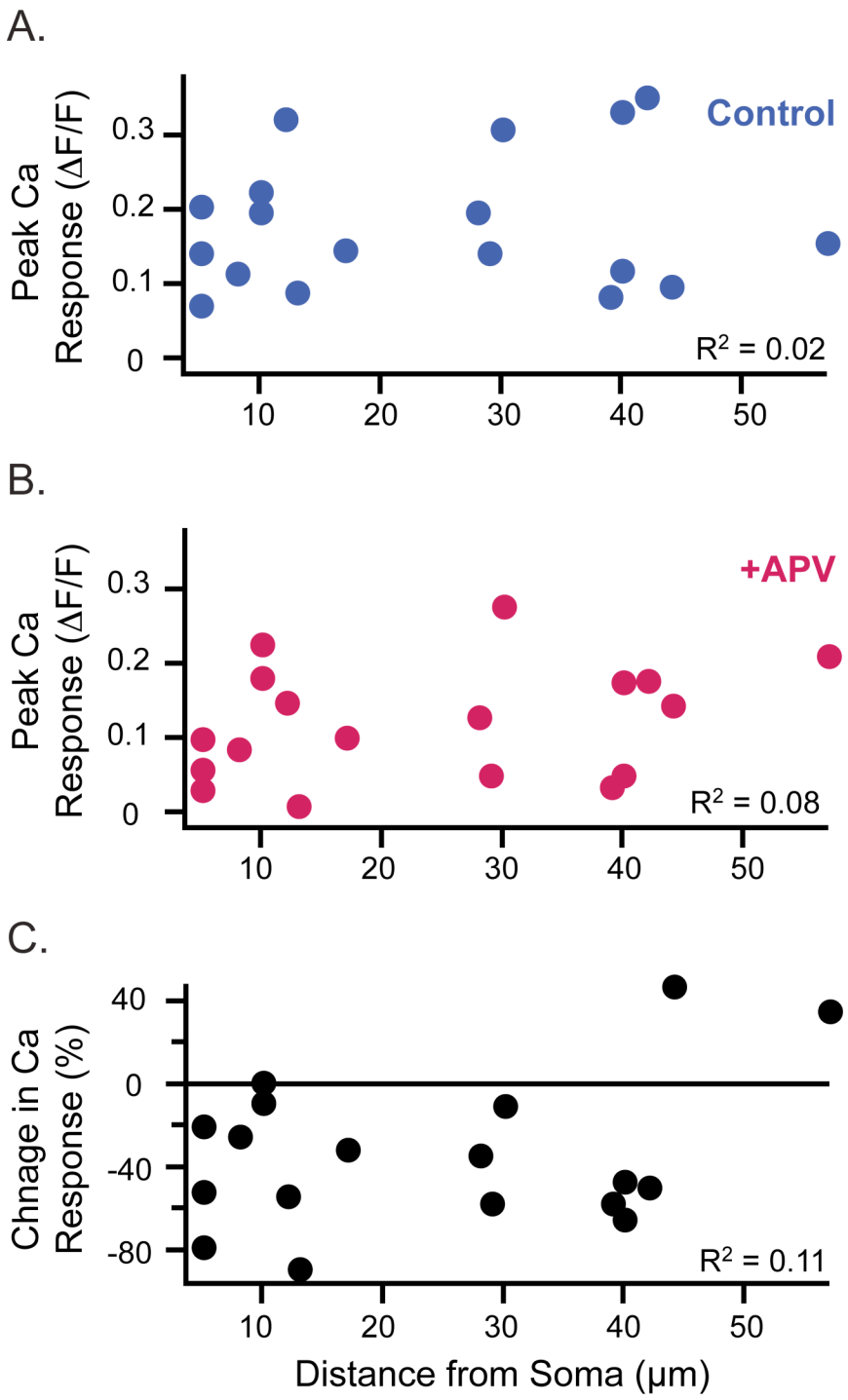

Figure 3: No correlation between soma-dendritic distance and NMDAR contribution
Soma-dendritic distance of dendritic Ca^{2+} response did not influence peak amplitude in control (A) or APV (B) conditions or NMDAR contribution to Ca^{2+} response (C).

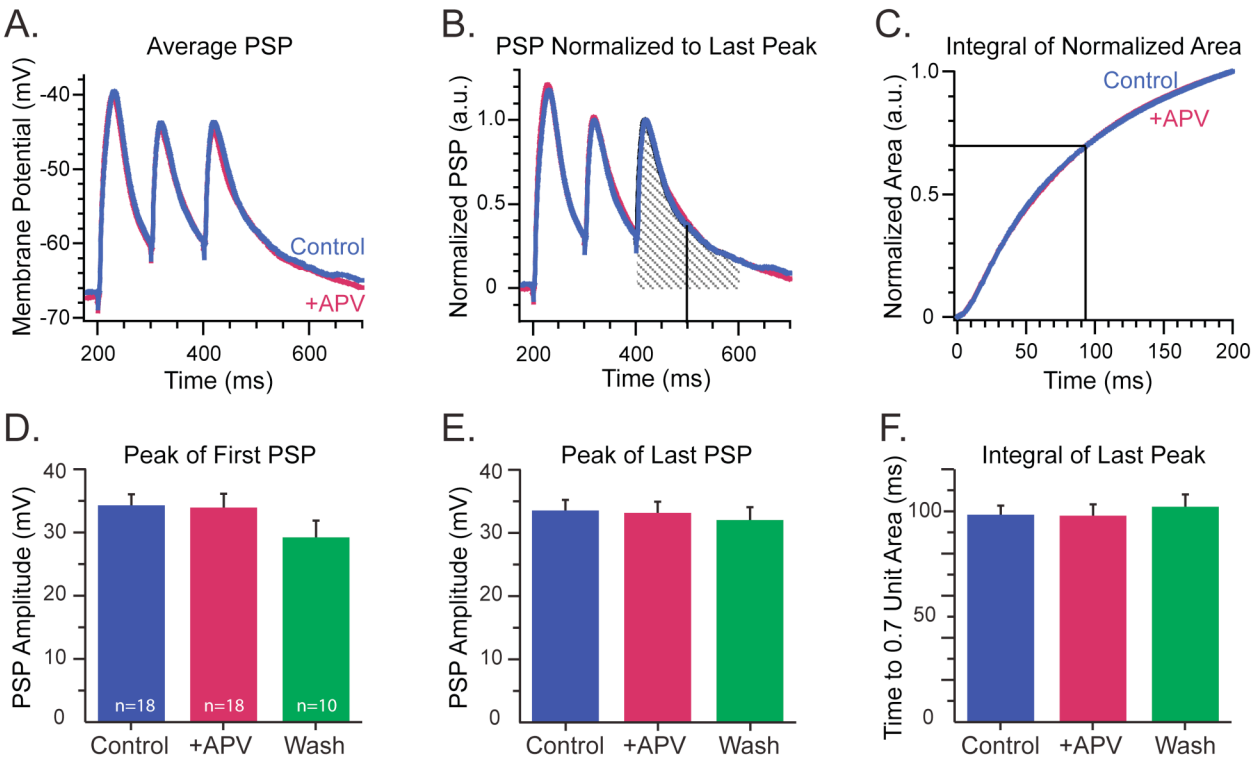

Figure 4: Somatically recorded synaptic potentials are not affected by APV.
A-C. Affect of APV on decay time determined by normalizing the average PSP (A) to the last peak (B), calculating the unit area of the last PSP and comparing the time to reach 0.7 unit area in control and drug conditions (C).
D-F. Peaks of first (D) and last (E) PSPs and the integral of the last peak (F) are consistent throughout recordings.

34.1±1.89mV; +APV: 33.8 ±2.83mV; Wash: 29.0±2.68mV; control vs APV p=0.8; APV vs wash p=0.9, n=18, paired ttests, Fig 4d). We also measured the amplitude of the last PSP because a decrease in NMDAR contribution to the decay phase might manifest itself as a decrease in summation of successive PSPs that would be observable as a decrease in the amplitude of the last PSP. Like the amplitude of the first PSP, the amplitude of the last PSP was consistent across conditions (Control: 33.4±1.9mV; +APV: 33.0±1.9mV; Wash: 31.8±2.2; control vs APV p=0.8; APV vs wash p=0.8, Fig 4e).

Since nonlinear conductances are present in current clamp recordings, changes in decay kinetics could not be calculated by fitting single or double exponentials to the decays of the electrical responses. Therefore, we elected to measure decay kinetics through an alternative method. This method measures the time it takes to pass 70% of the unit area under the last peak in the train. We calculate this by normalizing the area across a 200ms time window and integrating this value. We then find the time point when this integral reaches 0.7 of the unit area (Fig 4b,c). Using this method, we found that there was no change in the decay kinetics following application of APV (control 97.9±4.85ms; +APV 97.4±5.96ms; wash 101.7±6.44ms; control vs APV p=0.838; APV vs wash p=0.099, paired ttests; Fig 4f).

The data presented here provide experimental evidence for the ability of developing GABA/glycinergic synapses to elicit Ca^{2+} influx via a mechanism other than VGCC activation: that is via NMDARs. These results also show that under experimental conditions with depolarizing E_{revCl}, MNTB inputs are able to access NMDAR mediated Ca^{2+} influx in LSO principal neurons from P4-7 aged mice (GABA/glycine action switches polarity ~P4). However, this raises the question of whether MNTB-LSO inputs can access NMDAR signaling pathways when physiological GABA/glycinergic conductances are present.

B. Somatic Ca^{2+} responses under physiological Cl^- conditions

In the next experiments, we addressed the question of whether MNTB stimulation *alone* could elicit Ca^{2+} influx via NMDARs in LSO principal neurons from animals spanning the depolarizing-hyperpolarizing period of GABA/glycinergic conductances. To preserve the native intracellular Cl^-, we bulk-labeled the brainstem slice with the membrane-permeable Ca^{2+} indicator, Fura-2AM (Fig 5a). The potential for MNTB inputs to elicit NMDAR mediated Ca^{2+} responses, as well as the connectivity of the imaged neurons with the MNTB, was established by starting our experiments in Mg^{2+}-free (0Mg) ACSF. Robust Ca^{2+} responses to MNTB stimulation were found in neurons from animals of all experimental ages (P1-8) that were greatly attenuated or abolished, reversibly, with APV (Fig 5b, upper traces; Fig 7c). These data demonstrate that in 0Mg conditions, NMDARs can be activated regardless of the polarity of GABA/glycinergic conductances.

1. Developmental increase in NMDAR-elicited Ca^{2+} responses: We found that the peak Ca^{2+} responses in the 0Mg condition were significantly larger in neurons from the older age group (P4-8) than those from the younger group (P1-3 -ΔF/F = 0.18±0.05, n=57 cells, 5 animals; P4-8: 0.27±0.06, n=54 cells, 8 animals; $p<0.0001$, KS-test; $p<0.005$, ttest; Fig 6a). The average resting fluorescence did not change across age groups in these experiments (average resting fluorescence (a.u.) P1-3 = 1094±46; P4-8 = 1126±34, $p>0.3$, ttest). Thus, the increase in peak amplitude is not a result of a smaller 'F' in the ΔF/F calculation. Rather, we propose that there is a developmental increase in the ability of NMDARs to increase somatically recorded Ca^{2+} responses either: (1) directly via developmental change(s) in glutamatergic conductances at MNTB-LSO synapses resulting in increased Ca^{2+} influx through APV-sensitive Ca^{2+} channels or (2) indirectly via developmental changes in the excitability of LSO dendrites, perhaps enabling more action potentials (APs) per stimulus train and/or permitting more Ca^{2+} influx through activation of VGCCs with back-propagating action potentials.

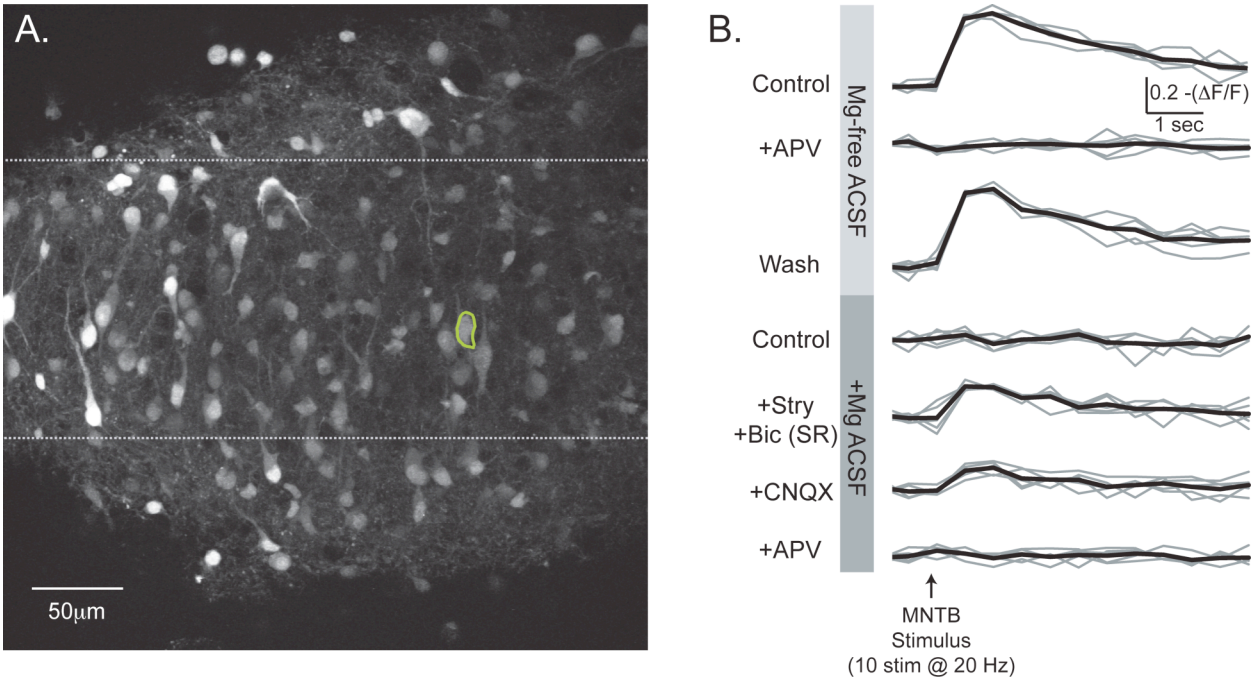

Figure 5: Somatic Ca^{2+} responses
A. Example of Fura2-AM stained LSO neurons.
B. Somatic Ca^{2+} responses from circled cell in A for 7 experimental conditions. Average of 5 trials/condition in black. In last 3 conditions, drugs applied additively.

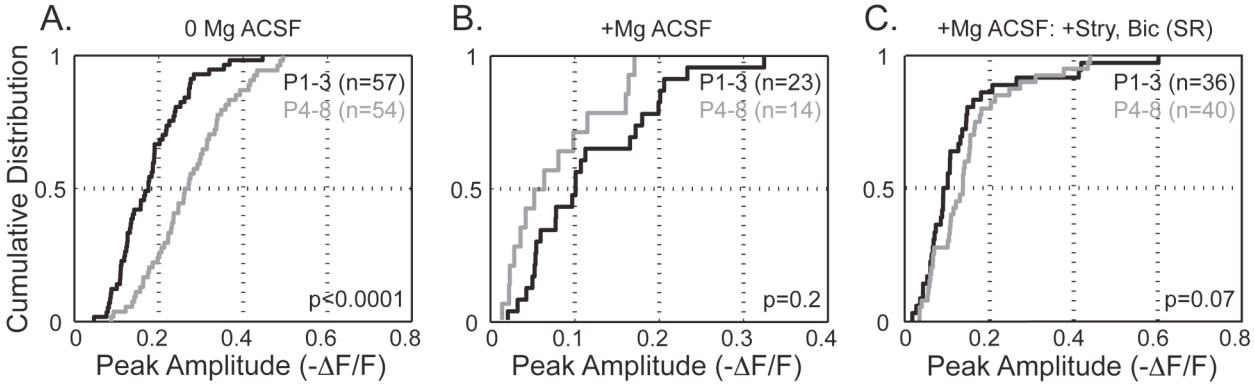

Figure 6: MNTB-elicited somatic Ca^{2+} responses recorded in 0Mg (A) increase during the first postnatal week. However, responses recorded in +Mg with (B) or without (C) GABA/glycinergic conductances are no different developmentally.

2. Mg^{2+}-sensitive Ca^{2+} responses: We next investigated the effect of normal Mg^{2+} ACSF (1.3mM) on these Ca^{2+} responses. Under physiological Mg^{2+} conditions, Ca^{2+} responses were abolished in most of the neurons regardless of age 34/57: 61% and 41/54:74% of neurons in P1-3 and P4-8 age groups, respectively; Fig 7c). The percentage of responsive cells was not statistically different between age groups for any condition ($p>0.08$, Fisher's exact test). Responses remaining in normal Mg^{2+} (+Mg) were greatly reduced compared with the 0Mg control conditions (P1-3: 47.5±6.6% of 0Mg control, n=23 cells, $p<0.0001$, paired ttest; P4-8: 25.8±5.2%, n=13 cells; $p<0.0001$, Fig 7Ai,Bi), consistent with previous findings demonstrating Mg^{2+} block at NMDARs in the LSO (Ene et al. 2003).

Adding Mg^{2+} had similar effects on Ca^{2+} responses to adding APV in 0Mg ACSF. Specifically, for each age group, the same percentage of cells that was responsive in 0Mg control was responsive in both of these experimental conditions (+APV/0Mg and +Mg; P1-3: 23/40: 40% of cells responsive in each condition; P4-8: 13/54: 24% and 14/54:26% of cells responsive in each condition, respectively; Fig 7c). In cells responsive in both conditions, the magnitude of the elicited responses was similar ($-\Delta F/F$ P1-3: +APV/0Mg = 0.122±0.016; +Mg = 0.137±0.019, n=16, $p>0.15$; P4-8: +APV/0Mg = 0.096±0.023; +Mg = 0.104±0.024, n=7, $p>0.7$, Fig 7Aii,Bii). These results suggest that *somatic,* APV-sensitive Ca^{2+} responses (activated by either sub- or supra-threshold inputs) are not -or rarely- found under physiological Cl^- and Mg^{2+} conditions, at any age studied. However, these data do not address whether *dendritic* APV-sensitive Ca^{2+} responses (activated by subthreshold inputs) can be elicited by MNTB inputs under similar ACSF conditions.

3. GABA/glycinergic shunting of Ca^{2+} responses: Previous studies have found that even depolarizing GABA/glycinergic activity can shunt excitatory responses by increasing the membrane conductance (Staley and Mody 1992; Hyson et al. 1995; Lu and Trussell 2001). To assess whether similar shunting is occurring in our system, we examined Ca^{2+} responses in the absence of ionotropic glycine (GlyRs) and GABA ($GABA_A$) receptor activation. When GlyRs and $GABA_A$s are blocked with Strychnine

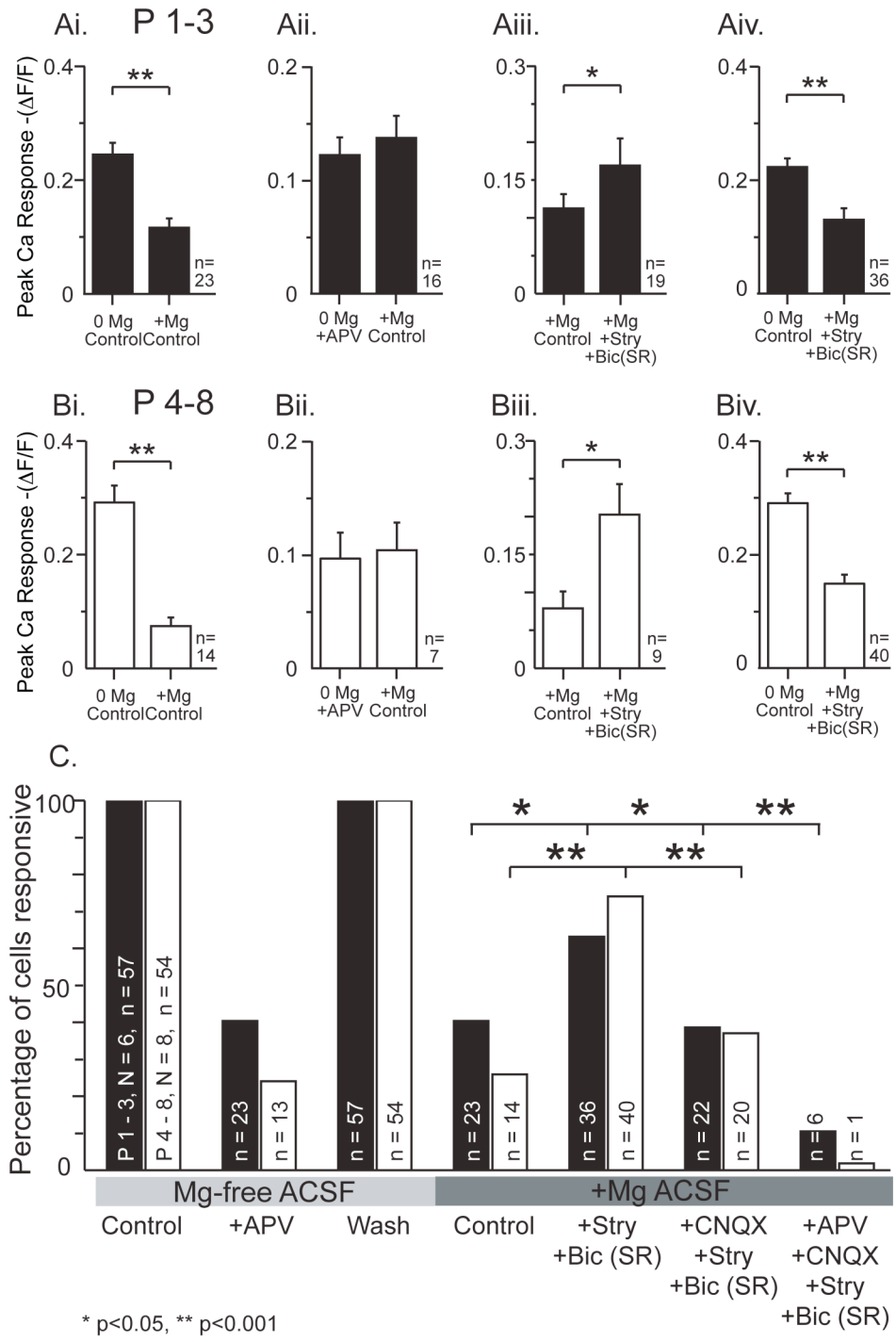

Figure 7: Changes in peak amplitudes of responsive cells.
A-B. Average responses from cells responsive in both conditions being compared.
C. Percentage of cells responsive in each experimental condition for cells from P1-3 (black) and P4-8 (white) animals. Statistical differences between groups ascertained with Fisher's exact test.

(Stry) and Bicuculline (Bic) or SR95531 (SR)), respectively, responses reappeared in many cells: the percentage of cells responsive in 0Mg control responsive in +Stry/Bic(SR) at P1-3 was 63.2% (36/54 cells); and at P4-8, 74.1% (40/54 cells, Fig 7c). Furthermore, blocking GABA/glycinergic conductances increased the Ca^{2+} response amplitude as compared with the +Mg condition in the subset of cells active in both conditions (-ΔF/F: P1-3: +Mg = 0.112±0.019; +Stry/Bic(SR)/Mg=0.169±0.036; 19/54 cells, $p<0.05$; P4-8: +Mg = 0.079±0.022; +Stry/Bic(SR)/Mg=0.203±0.040; 9/54 cells, $p<0.02$, paired ttests, Fig 7Aiii,Biii). These results support the idea that GABA/glycinergic conducantces shunt a glutamate-elicited Ca^{2+} response, even when GABA/glycinergic conductances are depolarizing with E_{evCl-} between -30 to -50mV at P1-3 (Kullmann and Kandler 2001).

The average response amplitudes for cells responsive in +Mg ACSF with GlyR/$GABA_A$s blocked were still smaller than those found in 0Mg ACSF conditions (-ΔF/F: P1-3: 0Mg-control=0.222±0.015; +Stry/Bic(SR)/Mg= 0.130±0.020; n=36 cells, $p<0.001$; P4-8: 0Mg-control=0.290±0.017; +Stry/Bic(SR)/Mg= 0.148±0.016; n=40 cells, $p<0.0001$, Fig 7Aiv,Biv). Thus, even with GABA/glycinergic conductances blocked in normal Mg^{2+} conditions, the glutamatergic Ca^{2+} responses still cannot reach their full potential, observed in 0Mg conditions.

Interestingly, as compared to the developmental increase in APV-sensitive Ca response observed in 0Mg, the amplitudes of glutamatergic Ca^{2+} responses observed under +Mg and +Mg with Stry/Bic(SR) conditions were similar in both age groups (-ΔF/F: +Mg P1-3=0.116±0.016, n=23 cells; P4-8=0.074±0.015, n=14 cells, $p>0.2$; +Stry/Bic(SR)/Mg P1-3=0.129±0.020; n=36 cells, P4-8= 0.148±0.016; n=40 cells, $p>0.07$, KS test Fig 6b,c). Thus, while the potential to elicit NMDAR-mediated Ca^{2+} responses is greater in the older (P4-8) age group, the ability to elicit these responses under physiological Mg^{2+} conditions is weaker in the older as compared with the younger (P1-3) age group. These results suggest that there are more 'silent' or NMDAR only MNTB-LSO synapses and/or a stronger Mg^{2+} block of NMDARs in the older (P4-8) age group because

4. Isolation of glutamatergic Ca^{2+} responses: Although AMPARs are impermeable to Ca^{2+} at this age (P1-8 (Ene et al. 2003)), AMPARs could contribute to an NMDAR mediated Ca^{2+} response through relief of the Mg^{2+} block. In support of this, subsequent to blocking NMDARS, blocking AMPARs with CNQX eliminated Ca^{2+} responses in 40-50% of the neurons responsive with GlyR/$GABA_A$s and attenuated the Ca^{2+} response in the remaining neurons (P1-3, $-\Delta F/F$: +Stry/Bic(SR)/Mg=0.164±0.03; +CNQX/Stry/Bic(SR)/Mg=0.134±0.03; n=22 cells, $p<0.005$; P4-8: +Stry/Bic(SR)/Mg=0.197±0.02; +CNQX/Stry/Bic(SR)/Mg=0.133±0.02; n=20 cells, $p<0.0005$). The remaining responses were predominantly mediated by NMDARs: application of APV eliminated responses in most cells (P1-3: 16/22 cells; P4-8: 19/20 cells) and reduced the amplitude of the responses in the remaining cells (P1-3, $-\Delta F/F$: +CNQX/Stry/Bic(SR)/Mg=0.124±0.04; +APV(CNQX/Stry/Bic(SR)/Mg)=0.092±0.03; n=6 cells, $p<0.05$; P4-8: +CNQX/Stry/Bic(SR)/Mg=0.122±0.03; +APV/CNQX/Stry/Bic(SR)/Mg=0.045±0.04; n=1 cell). The Ca^{2+} responses persisting in those seven cells under conditions with the four major classes of ionotropic receptors blocked are likely mediated by metabotropic receptors, perhaps through mGluR activation of TRP-like Ca^{2+} channels (Ene et al. 2003; Ene et al. 2007).

The data presented here suggest the presence of at least a subpopulation of NMDARs in developing LSO neurons that are Mg^{2+}-insensitive. The Mg^{2+}-insensitive NMDARs could then provide local depolarization that could unblock Mg^{2+}-sensitive receptors in a feed-forward manner. However, this would be in contrast to previous findings showing Mg^{2+}-sensitivity of NMDARs to NMDA (Ene, et al. 2003). Thus these data may alternatively indicate that electrical stimulation of the MNTB-LSO fibers elicits modulation of NMDARs, perhaps through activation of Group II mGluRs (Tyszkiewicz et al. 2004), which are known to be present in LSO neurons (Ene et al. 2003; Nishimaki et al. 2007).

IV. DISCUSSION

During the period of functional refinement (Kim and Kandler 2003), developing inhibitory neurons in the auditory brainstem release three different neurotransmitters: glycine, GABA, and glutamate (Gillespie et al. 2005). We hypothesized that the functional significance of glutamate release is to endow inhibitory neurons with the ability to utilize NMDAR triggered Ca^{2+} signaling cascades to selectively strengthen and eliminate synaptic inputs. In this study, we determined that NMDARs could contribute to Ca^{2+} responses under conditions that maximize the ability for GABA/glycinergic conductances to relieve Mg-block of NMDARs by altering the intracellular Cl^- levels. We then defined experimental conditions under which NMDAR mediated Ca^{2+} responses could be elicited under physiological Cl^- conditions. Taken together, these results detail a potentially powerful mechanism by which inhibitory topographic undergo refinement, namely through the co-release of glutamate and activation of NMDARs.

A. NMDAR mediated Ca^{2+} influx at dendritic MNTB-LSO inputs

Similar to many forms of plasticity at excitatory synapses (see review (Cavazzini et al. 2005)), many forms of plasticity at inhibitory synapses are dependent on activation of NMDARs (Stelzer et al. 1987; Grunze et al. 1996; McLean et al. 1996; Morishita and Sastry 1996; Wang and Stelzer 1996; Ouardouz and Sastry 2000; Marsden et al. 2007; Nugent et al. 2007). The mechanisms by which $[Ca^{2+}]_i$ increases, and not just absolute increases in $[Ca^{2+}]_i$, may have consequences for the induction of plasticity (Bender et al. 2006; Nevian and Sakmann 2006). At immature, depolarizing GABAergic synapses in

the hippocampus, bidirectional plasticity has been observed in which the direction of plasticity is dependent on whether NMDARs have been activated or not (McLean et al. 1996). In the deep cerebellar nucleus, high frequency simulation elicits NMDAR dependent LTP (Ouardouz and Sastry 2000) and lower frequency stimulation elicits VGCC dependent LTD (Morishita and Sastry 1996). It therefore follows that by eliciting Ca^{2+} influx through NMDARs, developing MNTB-LSO inputs could access plasticity pathways that are inaccessible when Ca^{2+} enters through VGCCs, as occurs when GABA/glycine are depolarizing in the LSO (Kullmann et al. 2002), and thus could directly influence the induction of plasticity at these synapses.

Activation of NMDARs has proven to be crucial in the refinement of excitatory projections within topographic maps in multiple sensory systems, including the visual (Cline et al. 1987) and somatosensory (Fox et al. 1996; Iwasato et al. 2000). When NMDAR activity is disrupted during refinement, the patterning and segregation of projections is blurred and incomplete, and excessive branching of dendrites and axons and increase in synapse densities are observed. Alternatively, when NMDAR activity is amplified through exogenous application of NMDA, patterning and segregation is sharpened and more decisive borders are formed, and reduced branching and synapse densities are observed (Cline and Constantine-Paton 1990; Colonnese et al. 2005; Lee et al. 2005). The overlap in the developmental age when the MNTB-LSO tonotopic map is markedly refined and glutamate is released at MNTB-LSO synapses eliciting Ca^{2+} influx via NMDARs suggests that NMDAR signaling might also be pivotal in the refinement of inhibitory projections within topographic maps.

Since glutamate co-release at MNTB-LSO synapses persists past the developmental change in the Cl^- reversal potential, one possible function for glutamate co-release might be to maintain a certain level of excitability in the circuit by driving the postsynaptic LSO neuron closer to threshold. However, we found that application of APV did not significantly reduce the amplitude of somatically recorded PSPs while it did significantly reduce the Ca^{2+} response, which is consistent with a previous study indicating that even in 0Mg ACSF, current flux through glutamatergic receptors was a small fraction of total current flux (Gillespie et al. 2005). These data further support our driving hypothesis that glutamate co-release at developing inhibitory inputs endows

these inputs with access to Ca^{2+} signaling cascades initiated by NMDAR activation that are fundamental to plasticity at excitatory inputs. Thus, the functional target of glutamate co-release appears to be in sculpting the input and not the output of LSO neurons.

A potential target of glutamatergic signaling in the developing MNTB-LSO pathway could be to mediate the subcellular reorganization of the inhibitory inputs. An immunohistochemical study found that during LSO development, the pattern of glycine receptors shifts from a diffuse pattern distributed across the soma and dendrites to a punctate-like pattern that is concentrated perisomatically (Friauf et al. 1997). Developmental removal of dendritic glycinergic synapses was also observed at LSO's sister nucleus, the medial superior olive (Kapfer et al. 2002). These developmental studies are complemented by electron microscope studies of LSO neurons in juveniles and adults demonstrating that the majority of inhibitory inputs to LSO neurons are found proximal to excitatory inputs (Cant 1984; Helfert et al. 1992). These studies suggest that single MNTB-LSO inputs are eliminated or strengthened based on their subcellular location. If the mechanisms underlying the 'direction' synaptic plasticity were reflected in the means of Ca^{2+} influx, we would expect a dendritic gradient reflecting the contribution of different methods of Ca^{2+} influx, e.g. NMDARs. We did not, however, observe such a gradient either because one is not present or only observable at more distal dendrites or at inputs on secondary dendrites: we investigated responses within the first 50µm of the dendritic arbor and the responses were predominantly on the principal dendrite.

A recent study from our laboratory described a positive correlation between the distance from the soma and the amplitude of Ca^{2+} responses elicited by back propagating action potentials (Kullmann and Kandler 2008). They posited that the Ca^{2+} response amplitudes increase as a result of the dendrites tapering with distance from the soma. We, however, did not observe a correlation between the distance from the soma and the amplitude of Ca^{2+} responses elicited by synaptic stimulation. Several explanations could account for this. First, in the previous study, data from the same cell were used to calculate the correlation, whereas in this study, data from 18 different cells were pooled. Second, in this study, there is a positive trend between the somatic distance and Ca^{2+} response amplitude over the first 30 µm, but there are several outliers at 40-50 µm from the soma. Thus, additional data points taken at the more distal

locations might compensate for the outliers and provide a positive correlation across the population of responses. Finally, it may not be appropriate to expect a correlation between somatic distance and synaptically elicited Ca^{2+} response amplitudes because a correlation exists between somatic distance and back-propagating action potential-elicited Ca^{2+} response amplitudes. The regenerative aspect of back propagating action potentials provides a more uniform voltage along the dendrites and enables the comparison of Ca^{2+} responses elicited a different somatic distances. Synaptic inputs, on the other hand, are not necessarily uniform in size and strength along the dendrite, so the variability in the inputs will add to the variability in the observed Ca^{2+} responses. A different experimental design is needed to more accurately determine whether a correlation exists between somatic distance and Ca^{2+} response amplitude: glutamate, GABA, and glycine should be systematically uncaged along the dendrites of individual neurons and the elicited Ca^{2+} responses recorded.

B. Somatic Ca^{2+} responses

Our first approach to the question of whether MNTB-LSO synapses can elicit NMDAR mediated Ca^{2+} influx under conditions of physiological Cl^- conditions was to investigate somatic Ca responses in Fura bulk-labeled slices. Although these somatic Ca^{2+} responses were measured in the absence of electrical recordings, we posit they were likely elicited by suprathreshold synaptic stimulation. The stimulus intensity used (800μA) could elicit APs with a single stimulus in other experiments when a cell was held in current clamp in 0Mg ACSF (Kalmbach and Kandler, unpublished observations) and in these experiments, we used a strong stimulus pattern of 10 pulses at 20Hz. Furthermore, responses across experimental conditions were similar in the 6 cells in which both somatic and dendritic Ca^{2+} responses were recorded (data not shown). These experiments, however, do provide valuable information regarding developmental changes and circumstances in which glutamate co-release elicits somatic Ca^{2+} responses.

We observed a developmental increase in the NMDAR-elicited Ca^{2+} response in the absence, but not the presence, of Mg^{2+}. This could result from a developmental increase in NMDAR-only synapses, which are functionally silenced and are awaiting subsequent elimination. The developmental increase we observed in the NMDAR-elicited Ca^{2+} responses in the 0Mg ACSF condition could result from developmental changes in the glutamatergic conductances at MNTB-LSO synapses or in the excitability of LSO dendrites. Immunohistochemical studies found a developmental increase in the staining pattern of VGluT3, the vesicular glutamate transporter expressed in MNTB neurons (Blaesse et al. 2005; Gras et al. 2005). In addition, electrophysiological studies demonstrated increases in NMDAR conductances in MNTB neurons until P11/12, after which time these conductances decreased (Joshi and Wang 2002). Alternatively, dendritic excitability could have increased developmentally. The number of APs elicited by a depolarizing current injection increases strikingly during the first postnatal weeks (Sanes 1993; Kandler and Friauf 1995), suggesting an increase in excitability [however, there is also a concurrent decrease in input resistance, suggesting a decrease in excitability (Kandler and Friauf 1995)]. Or the observed developmental increase in Ca^{2+} response is a combination of both changes. Further experiments investigating glutamatergic conductances in response to sub- and supra-threshold inputs during development could tease apart the biological basis of our observed developmental increase in NMDAR-elicited Ca^{2+} responses.

Depolarizing GABAergic conductances can have a net inhibitory effect (Staley and Mody 1992; Hyson et al. 1995; Lu and Trussell 2001). It was found that although stimulation of GABAergic fibers independently can elicit action potentials, when GABAergic and glutamatergic fibers are stimulated simultaneously, the spiking probability decreases significantly (Lu and Trussell 2001). In our experiments, we found that blocking GABA/glycinergic conductances consistently uncovered a glutamatergic Ca^{2+} response that was either absent or greatly attenuated in the presence of these conductances, even between P1-3 when GABA/glycinergic conductances are depolarizing in the mouse (Kullmann and Kandler 2001). A previous study from our laboratory demonstrated Ca^{2+} responses elicited by GABA and glycine application and stimulation of MNTB-LSO fibers in the presence of ionotropic glutamate blockers

(Kullmann et al. 2002). The data presented in this thesis do not contradict the previous work. We also observed Ca^{2+} responses that were mediated by GABA/glycinergic conductances: when Stry/Bic(SR) was applied, responses in 4/23 cells in the P1-3 group and 5/14 cells in the P4-8 group were abolished. Furthermore, as glutamatergic conductances were already blocked in the previous study when Stry/Bic was applied, the uncovering of glutamatergic Ca^{2+} responses would not be observable. In our experiments, the consistency with which Ca responses increased or reappeared following application of GABA/glycine receptor antagonists suggests that GABA/glycinergic conductances shunt a somatically-imaged glutamatergic Ca^{2+} response.

C. Conclusion

In summary, when GABA/glycinergic conductances are depolarizing, MNTB inputs can elicit local dendritic Ca^{2+} responses via NMDARs. However, MNTB inputs by themselves are unable to elicit *somatic*, APV-sensitive Ca^{2+} responses under conditions maintaining physiological Cl^- and Mg^{2+}, despite having the potential to elicit these Ca^{2+} responses. This may be because the somatic Ca^{2+} responses we recorded resulted from suprathreshold inputs that were attainable in the absence of either Mg^{2+} or GlyR/$GABA_A$ activation, while subthreshold, APV-sensitive Ca^{2+} responses might still be present along the dendrites or below our detection threshold. Nevertheless, the prominence of APV-sensitive Ca^{2+} responses under 0Mg conditions strongly suggests that there are physiological conditions under which APV-sensitive Ca^{2+} responses can be elicited.

From the data presented in this thesis, we propose two models that depict two different scenarios in which MNTB inputs could elicit NMDAR-mediated Ca^{2+} responses under physiological Cl^- and Mg^{2+} conditions. In the first model, activation of AMPARs by MNTB inputs provides a small region of depolarization that relieves the Mg^{2+} block at NMDARs, permitting localized NMDAR-mediated Ca^{2+} influx. This could occur either at

glutamate-only synapses or at the fringes of glutamate/GABA/glycinergic synapses (Fig 8a). In the second model, co-activation of the cochlear nucleus (CN) and MNTB inputs could provide relief of Mg^{2+} block for NMDARs activated by MNTB inputs (Fig 8b). This second model is particularly intriguing because it requires cooperativity between the binaural inputs to the LSO in order for MNTB inputs to activate NMDARs with their co-release of glutamate. This cooperativity provides a mechanism to align the tonotopic projections from the binaural inputs. Future experiments that investigate whether stimulating only the MNTB inputs can elicit NMDAR-mediated Ca^{2+} responses under physiological Cl^- and Mg^{2+} conditions will provide further insight into which model best describes how MNTB inputs utilize their potential to elicit NMDAR-mediated Ca^{2+} responses.

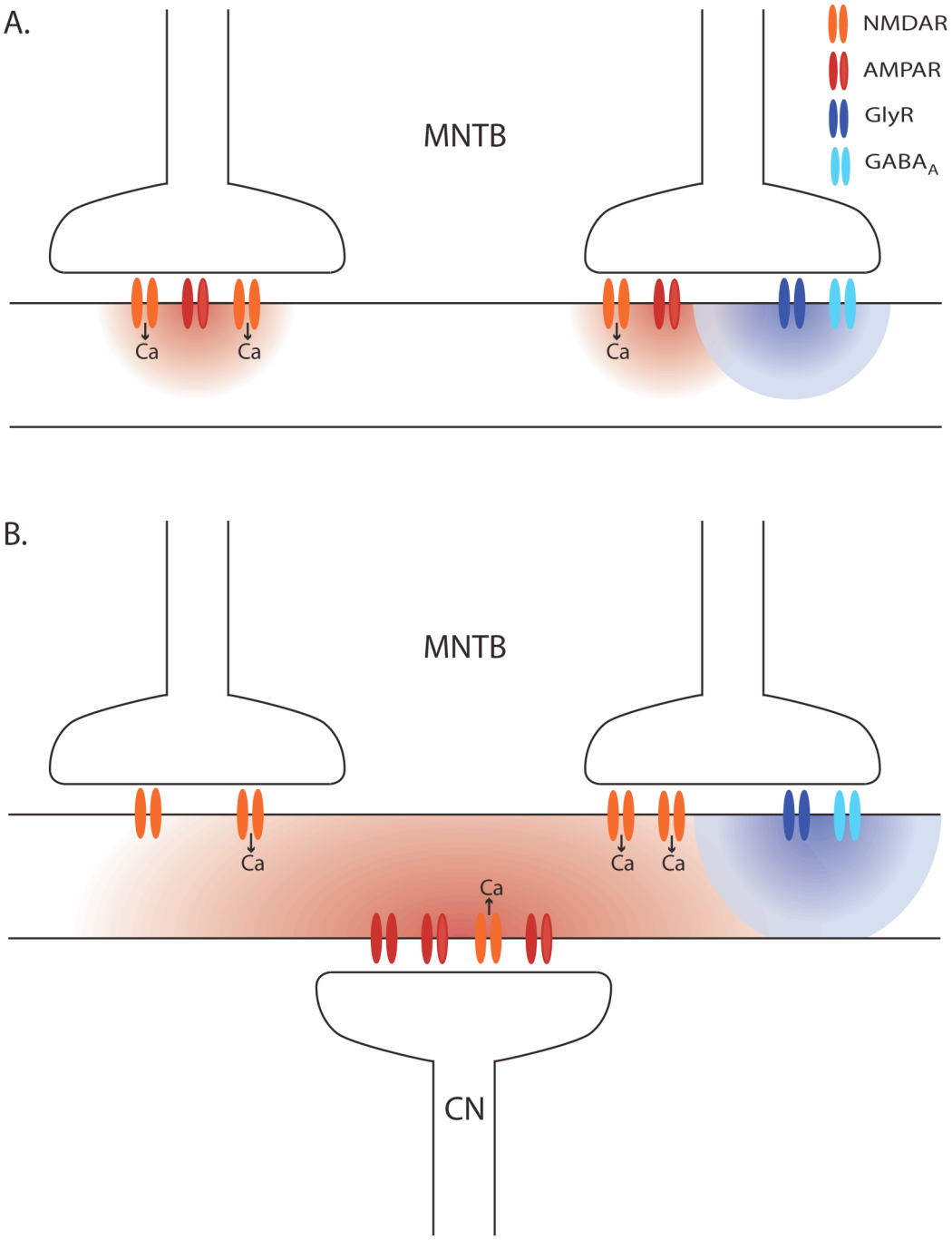

Figure 8: Possible physiological conditions under which MNTB-LSO inputs could elicit NMDAR-mediated Ca^{2+} responses, even when GABA/glycinergic conductances are hyperpolarizing.
A. MNTB-LSO elicited AMPAR activation creates small depolarized regions permitting Mg^{2+} unblock at NMDARs.
B. Coactivation of the excitatory CN-LSO inputs provide Mg^{2+} unblock for NMDARs activated at MNTB-LSO inputs.
Hot/cool colors represent dendritic depolarization/hyperpolarization.

APPENDIX: CONSTRUCTION OF A 2-PHOTON IMAGING SYSTEM

BACKGROUND

In 1931, Nobel laureate Maria Göppert-Mayer predicted that in the same quantum event one atom or molecule could absorb two photons simultaneously or within a temporal window of 0.1 femtoseconds (Göppert-Mayer 1931). Experimental validation, however, necessitated the development of laser sources, in particular the development of ultrafast lasers, which came into fruition in the 1960's (Wise 1999). While the advantages of utilizing this nonlinear phenomenon for imaging thin optical sections in microscopy was realized in the late 1970's, the practical implementation of two-photon microscopy required further development of laser sources that could provide mode-locked, high-peak-power femtosecond laser pulses (Diaspro and Sheppard 2002). Concurrent with the evolution of laser sources was the development of laser scanning microscopy. The marriage of these two areas finally occurred about two decades ago and the revolution of 2-photon fluorescence microscopy was born (Denk et al. 1990).

The predominant advantage of 2-photon over 1-photon microscopy is the reduction in phototoxicity and photobleaching that is inherent in the 2-photon excitation process. In 1-photon excitation, a single photon excites a fluorophore to a higher energy state and when that fluorophore relaxes back to the ground energy state, fluorescence emissions occurs (Fig A1a). Because energy is lost during the process of thermal relaxation, the emitted fluorescence has a longer wavelength than that used for excitation. Since most fluorophores emit blue-green wavelength light, the excitation wavelength required to excite these fluorophores is in the UV region of the light spectrum. However, prolonged exposure over the course of an experiment, for example,

to light of this intensity leads to photobleaching of the fluorophore and photo- and cell-toxicity. Additionally, since the absorption of only a single high-energy photon is required for excitation, photodamage can be inflicted not only at the focal plane but also on any molecule within the light path (Fig A1c).

In 2-photon excitation, on the other hand, the simultaneous absorption of two photons excites the fluorophore to the higher energy state (Fig A1b). Since the energies from the pair of photons work together to excite the fluorophore, the photons can have longer wavelengths. In addition to being less toxic to the cells, the longer wavelength (lower energy) photons are better able to circumvent obstacles and can penetrate deeper into tissue, which is a huge benefit for *in vivo* imaging. Furthermore, since the absorption of the 2-photons must occur virtually simultaneously, the likelihood of this phenomenon is only realistic at the focal plane of the objective, where the photon flux is the greatest (Fig A1d). Thus, fluorophores and DNA that are out of the focal plane will not bleach or be damaged. While 2-photon excitation can still be damaging within the focal plane, provided the duration and intensity of light exposure is kept to a minimum, extensive live-neuronal imaging experiments can be performed.

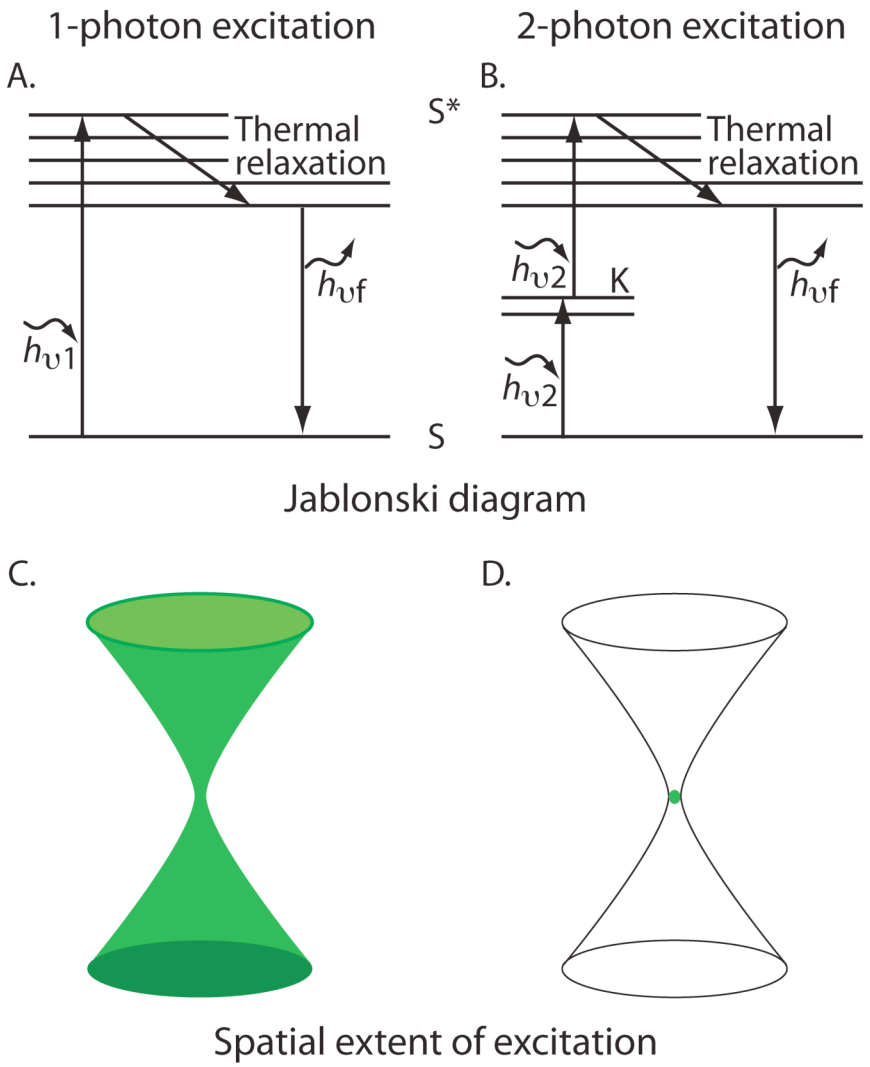

Figure A1: Differences between one- and two- photon excitation processes.

A,B. Schematic of Jablonski diagram depicting excitation under one- and two-photon absorption. S and S* are the ground and excited states, respectively. K is a virtual state that is transiently visited. Energy of photon absorbed in one-photon excitation (hv1) is approximately twice that of photons absorbed in two-photon excitation (hv2). Emitted fluorescence energy (hvf) is less than hv1 but greater than hv2.
C,D. Cartoons of the spatial extents of excitation for one- and two-photon excitations.

SELECTION AND ASSEMBLY OF COMPONENTS

In the following pages, I outline the considerations and choices I made in designing and building a 2-photon microscopy system.

Excitation Beam Path

Choice of Ti:sapphire laser: The two major commercial companies which supply femtosecond Ti:sapphire lasers are Coherent and Spectra Physics. We opted to purchase Coherent's Chameleon XR system for several reasons. The Chameleon laser systems have a significantly smaller 'footprint' than the systems supplied by Spectra Physics. Thus, we were able to fit the laser, necessary optics and microscope onto our existing 8'x4' air table. We specifically chose the Chameleon XR model because the output beam could be tuned over an extended range of wavelengths from 720-980nm.

Modulation of power: Only a small fraction of the available laser power (<5mW of the possible 1200mW) is necessary for – and is nontoxic to –imaging live neurons. While the optics along the beam path significantly reduce the laser power, the power still needs to be reduced even further. Although the power of the Chameleon XR can be changed, any significant deviation from the factory determined settings causes the laser to fall out of modelock, meaning that the laser is no longer pulsed at MHz frequencies. Also, once modelocking is lost, the system automatically resets the laser to be pumped at the high, pre-set level. Therefore, we chose to utilize two methods to reduce the laser

power to safe, neuron-friendly levels. The first phase of power modulation is performed by an adjustable half-wave plate coupled with a linear polarizing filter (Fig A2a). By changing the direction of the laser beam's polarization with the half-wave plate and selecting only the fraction of the laser beam that is polarized in the planar direction, we can significantly reduce the power of the beam. The second phase of power modulation is simply a pair of neutral density filters. Since the half-wave plate is adjustable, we can change the laser power during the course of the experiment. However, this adjustment is done manually so this power modulation system is not appropriate for dynamically changing the laser power, as would be desired when doing combined uncaging and imaging experiments. For those experiments, a computer controllable acousto-optic modulator is needed, but this is significantly more expensive.

Back-filling of objective: In order to minimize the longitudinal axis of excitation, the beam should fill the back of the objective, which will enable the full numerical aperture of the objective to be used. As the beam diameter is smaller than the back of the objective, to expand the beam diameter, we constructed a Keplerian telescope, which is composed of a pair of plano-convex lenses (Fig A2b).

Beam steering and other optical components in light path: Silver coated mirrors were used to steer the beam through the power modulation and telescope optics (Fig A2c). A periscope with a pair of these mirrors was used to bring the beam from the surface of the air table up to the laser scanning unit (Fig A3). Also in the light path is a pair of iris diaphragms for aligning the beam through the telescope (Fig A2d).

Additional modifications to confocal system: Our microscope and laser scanning unit were designed for shorter wavelength light than that used for 2-photon imaging. Therefore, we replaced the mirrors on the galvonmeters (which steer the beam across the image plane) and the microscope tube and scan lenses with infrared compatible components. We also replaced the dichroic mirror that the confocal unit used to separate the excitation from the emission light with a mirror.

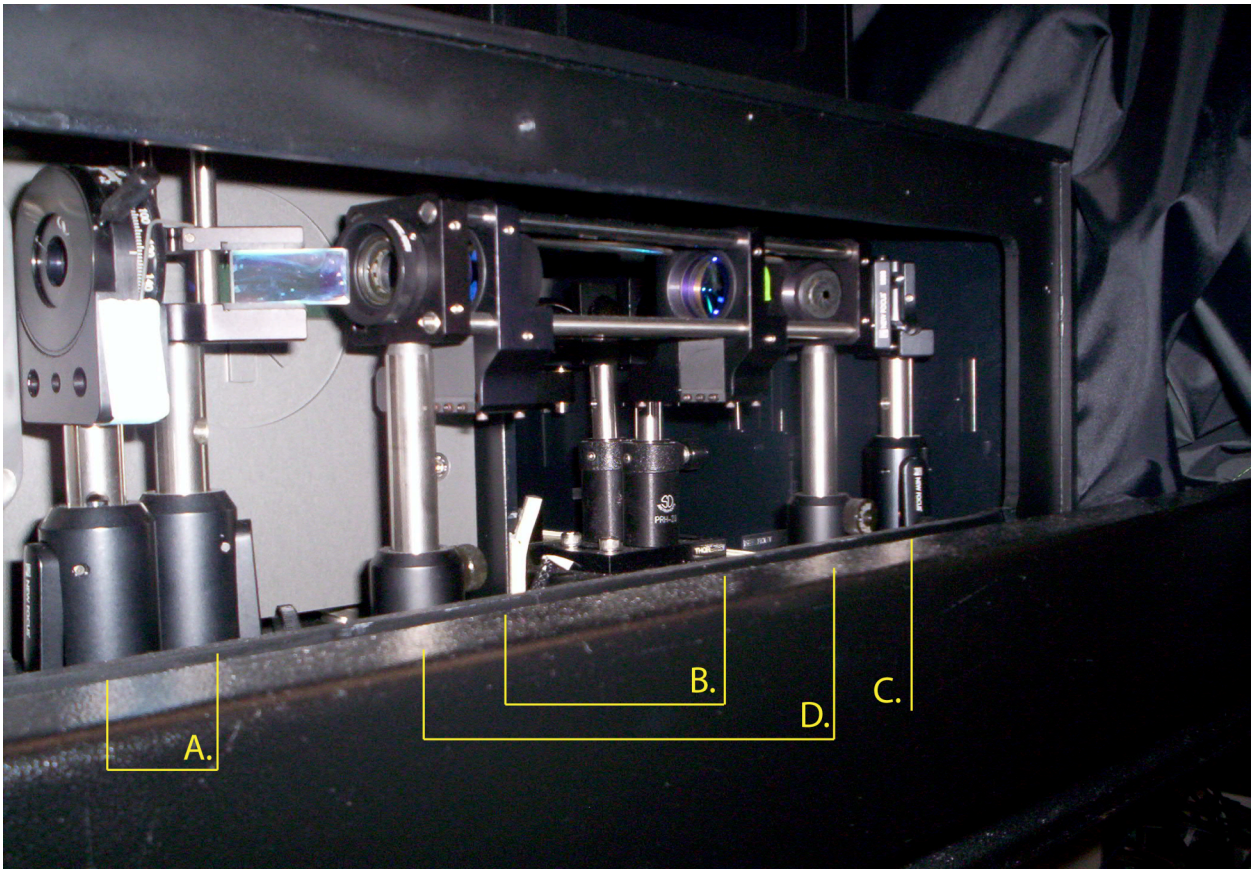

Figure A2: Optical components along excitation beam path.
A. Achromatic zero order quartz MgF2 half-wave plate (Newport 10RP52-2) and ultrafast laser thin film polarizer (Newport 11B00UP.25).
B. Keplerian telescope composed of plano-convex lenses (Thorlabs LA1131B and LA1134B with focal lengths of 50mm and 60mm, respectively).
C. Silver coated beam-steering mirror (New Focus nf5103).
D. Iris diaphragms (Thorlabs SM1).
Rigid components purchased from the various optics suppliers.

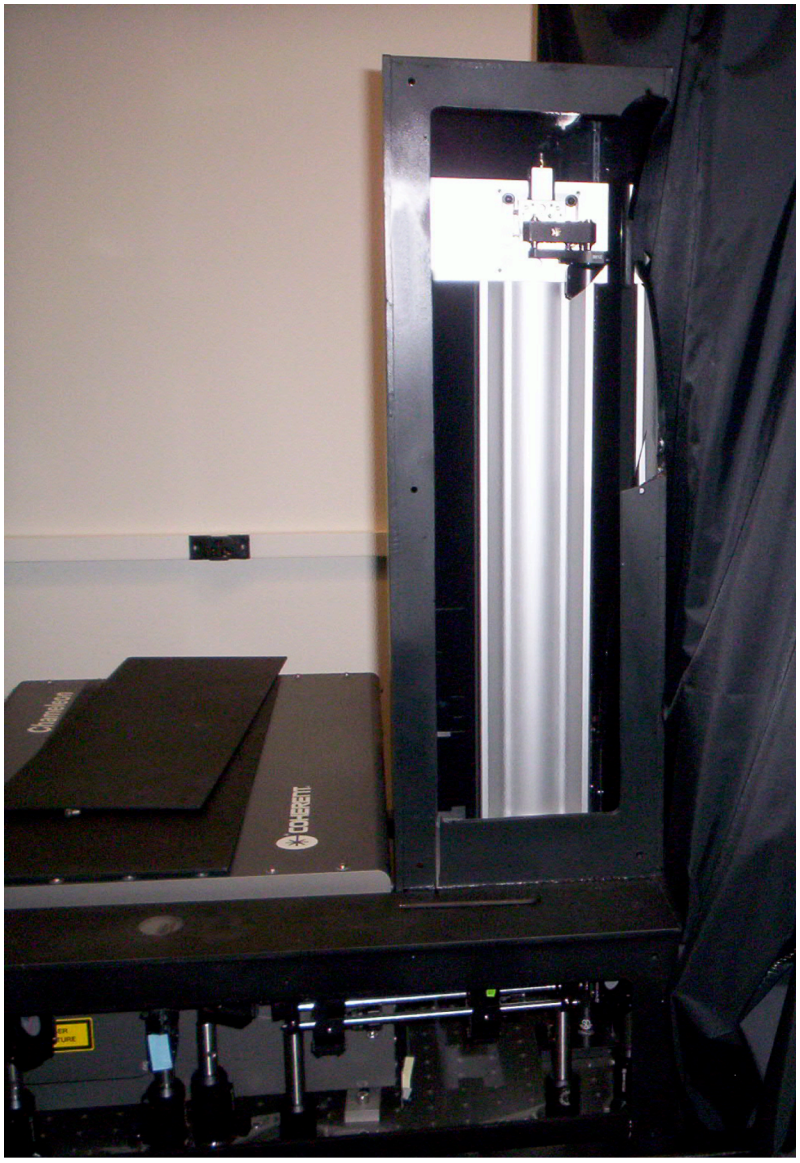

Figure A3: Image of periscope along excitation light path.
The laser beam was brought from the tabletop to the scan head via a pair of mirrors mounted to a Gimbal mount (New Focus 9812-K) via a 45deg adaptor (New Focus 9920). The mounts were attached to an x-translation stage (New Focus 9066X-M), which were in turn secured to carriers for the x95 profile tube (Linos carriers: 02 6421; tube: 02 6106). The entire periscope sits on top of a crossed roller translation stage (Siskiyou 200cr).
Note: only the upper mirror and carrier is visible in this image.

Detection of emitted fluorescence

Collection of epi-fluorescence light: Fluorescent light emissions that traveled back through the objective were steered towards the epi-fluorescence port of the microscope with a dichroic mirror (Chroma 675 dcxpxr) placed in the filter cube in this port. The back of this port was retrofitted with a custom-built photomultiplier tube (PMT) mount (Department of Cell Biology and Physiology and Pharmacology machine shop at University of Pittsburgh; Fig A4). Within the PMT mount, a blocking emissions filter (Chroma e700sp-2p) provided an additional safeguard against wayward laser light. The emissions beam was then split with a 45deg beamsplitter (Semrock* FF560-Di01) to separate the emissions from green and red emitting fluorophores. The red light was collected with a head-on PMT (Hamamatsu R6095P; Fig A4a), which collected the light via Köhler detection, meaning that the detector is placed in the back focal plane of the collector lens. A pre-amplifier circuit (Advanced Research Instruments Corp PMT-4) then readied the output for acquisition by the computer. The green light was collected with a side-on PMT (Hamamatsu R3896; Fig A4b) that was taken from the Olympus FluoView scanhead and which collected the light via critical detection, meaning that the light is focused onto the collection window of the PMT with a plano-convex lens (Thorlabs LA1951, f=1").

Collection of trans-fluorescence light: As emitted photons travel in all directions, we also collected emissions traveling through the condenser. Since our microscope model has a fixed arm (Olympus BX50WI), there was a limited amount of space to work with below the specimen stage (fig A5a). However, with careful planning and excellent

* Semrock filters have superior optical properties and are more reasonably priced than Chroma's filters, but were not on the market when we initiated assembly of this system. Furthermore, the lead time in acquiring their filters is substantially shorter (days vs. months) because they are not custom made with each order.

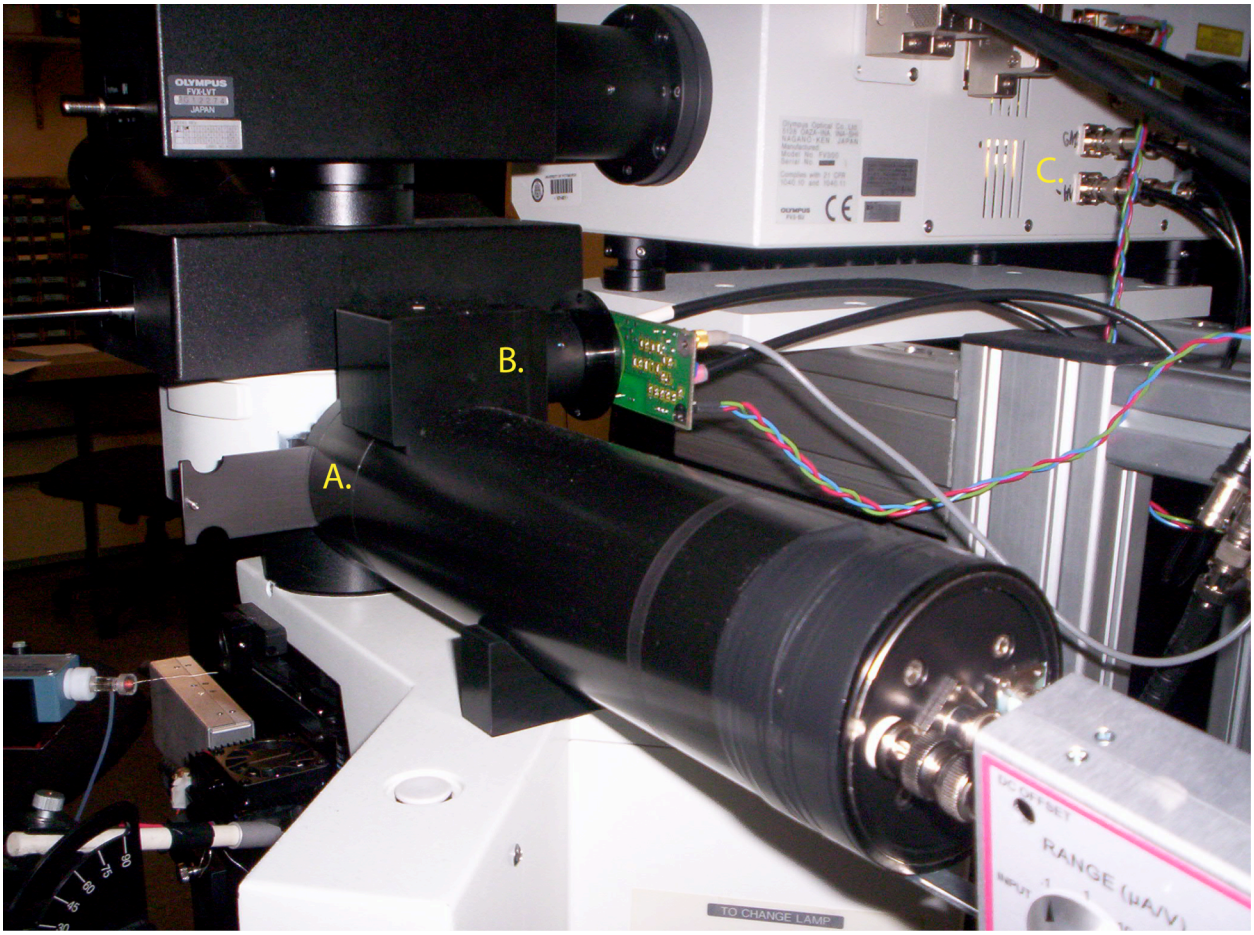

Figure A4: Epi-fluorescence PMTs
A. PMT tube enclosing optics and headon PMT.
B. Port enclosing sideon PMT.
C. Rear view of Olympus FluoView scanhead that was modified to provide power and control signals to these PMTs.

support from the machine shop, we were able to install a third PMT to collect the trans-fluorescence light. In order to maximize our collecting efficiency, we utilized a high N.A. oil condenser (N.A. 1.25, gift from Dr. Fred Lanni, Carnegie Mellon University; Fig A5b). The condenser screwed into a housing (Fig A5c) hosting an iris diaphragm that is very useful for bright-field illumination but is kept open during fluorescence imaging. The height of the condenser-iris block can be adjusted independently of the remaining optics in this light path in order to "Köhler" the bright-field illumination.

The emissions and excitation light are then separated with a dichroic mirror (Semrock FF665-Di01 assembled into a Zeiss filter cube; Fig A5d). As in the epi-fluorescence detection, the emissions were further filtered to remove any laser light from this light path (Semrock FF01-680/SP; Fig A5e). This is particularly important for trans-fluorescence detection because of the angle of the dichroic is perfect for redirecting the laser light along this path (the angle of incidence in the epi-fluorescence case is in the opposite direction). An additional filter selected for green as opposed to red fluorescence (Semrock FF01-510/84; Fig A5e). The emissions then passes through a collecting lens (Thorlabs LA1034, f=2.5"; Fig A5f), which focuses the light onto the PMT.

Between the collecting lens and the PMT is an electronic shutter (Melles Griot 04 ESC 131; Fig A5g). Several series of circuits time the opening of the shutter to coincide with the time when fluorescence imaging is being performed. The shutter is directly opened with the commercial controller (Melles Griot 04 ISC 850). This controller is triggered by a custom-built circuit (built by the Chemistry electronics shop at the University of Pittsburgh), which integrates the square-wave pulses sent by the imaging software (Olympus FluoView 300) during image acquisition.

The trans-fluorescence is detected by a high end, Peltier and fan-cooled PMT (Hamamatsu H7422; Fig A5h). The PMT is controlled with a custom-built circuit (Chemistry electronics shop) that enables the cooling elements and directs power to the PMT. This PMT has exquisite photon collecting properties (see Fig A6 for comparison of images collected by this PMT and the side-on PMT at the epi-fluorescence port).

The final [external] component of the emissions detection path is a custom-built circuit (Chemistry electronics shop) that adds the signals collected at this PMT and the

side-on PMT at the epi-fluorescence port. A special feature of this circuit is the ability to adjust the relative contributions from each PMT.

Environmental imaging conditions

The last set of considerations I will elaborate on is concerned with the environmental imaging conditions. An important mantra to remember when doing fluorescence microscopy in general and 2-photon microscopy specifically is: *every photon counts.* This is appropriate on the excitation end of things to minimize photodamage and on the emissions end to maximize the collection of photons. In order to eliminate as much noise from extraneous light as possible, we took some precautionary measures to isolate the emissions light path from ambient light. For example, the epi-fluorescence PMT housing was machined to be light-tight. As a rigid structure was ill-suited for the trans-fluorescence PMT housing, we sewed and constructed light-tight shields from black-out fabric (Fig A7). We also isolated the specimen plane from extraneous light by sewing and constructing an enclosing unit for the microscope (Fig A8b). Curtains separated the microscope setup and workspace from the rest of the laboratory. During experiments, room lights were turned off and indicator lights were covered with red cellophane and computer monitors were adjusted to emit only red light. In addition to isolating the system from extraneous light, it is also important to limit temperature fluctuations in the room as changes in temperature affect the output of the Ti:sapphire laser. Finally, for personal safety, we enclosed the excitation beam path in plexiglass painted black to prevent wayward laser light from damaging our eyes (Fig A8a).

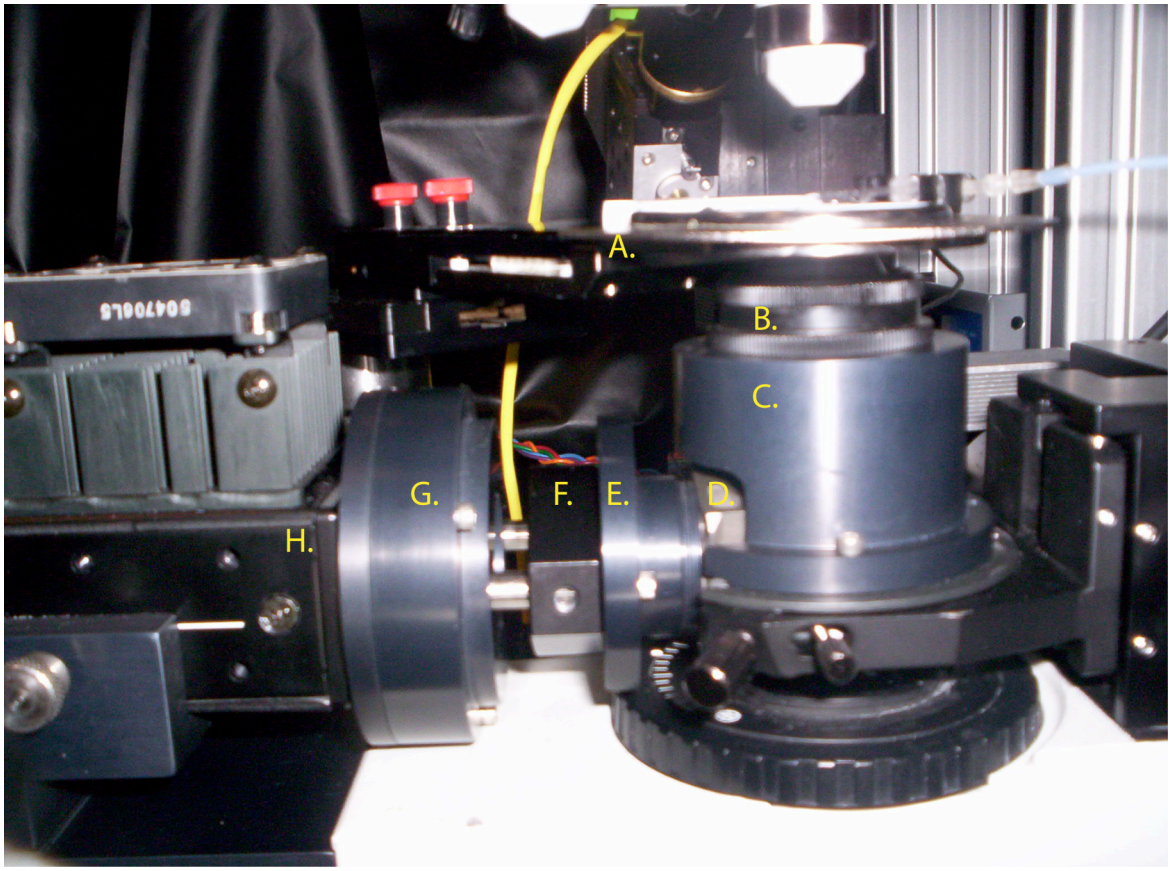

Figure A5: Image of trans-fluorescence light path. See text for details.

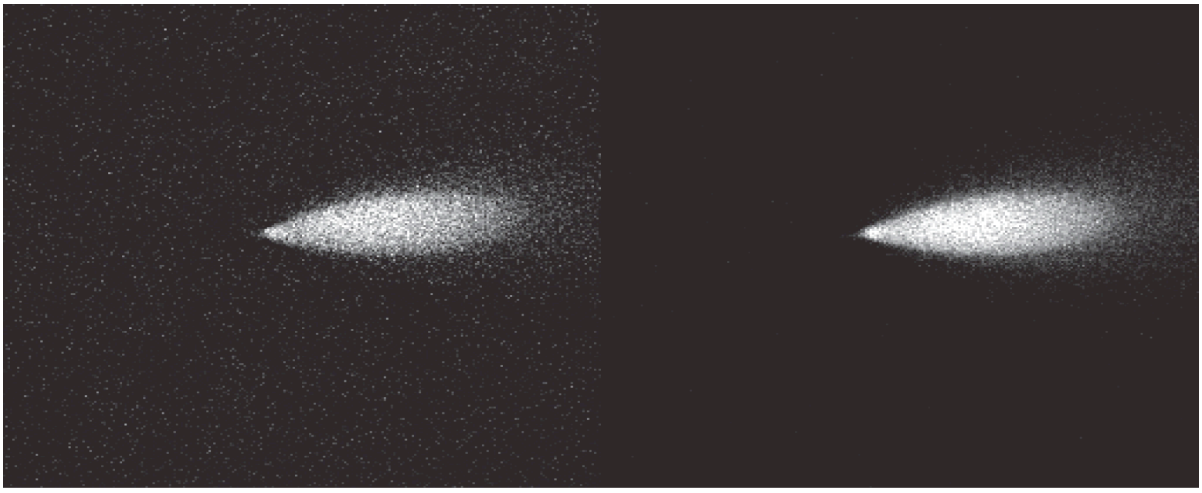

Figure A6: Comparison of fluorescence image acquired with the side-on PMT located at the epi-fluorescence port (left) and with the cooled PMT at the trans-fluorescence location (right).

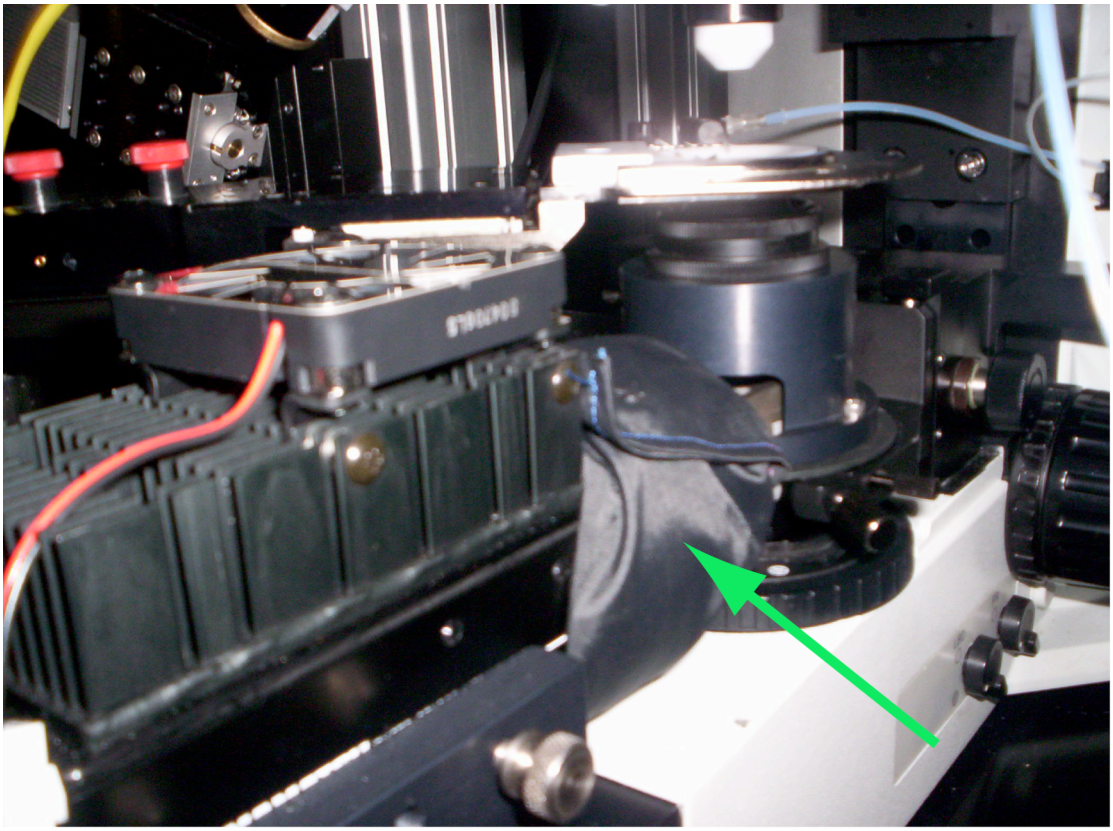

Figure A7: Inner light shield for trans-fluorescence emissions light path. An additional layer of shielding that fits around the condenser 'skirts' the components.

Figure A8: Light enclosures for the imaging system.

BIBLIOGRAPHY

Bender, V. A., K. J. Bender, D. J. Brasier and D. E. Feldman (2006). "Two Coincidence Detectors for Spike Timing-Dependent Plasticity in Somatosensory Cortex." J. Neurosci. **26**(16): 4166-4177.

Blaesse, P., S. Ehrhardt, E. Friauf and H. G. Nothwang (2005). "Developmental pattern of three vesicular glutamate transporters in the rat superior olivary complex." Cell and Tissue Research **320**(1): 33-50.

Boudreau, J. C. and C. Tsuchitani (1968). "Binaural interaction in the cat superior olive S segment." J Neurophysiol **31**(3): 442-54.

Cant, N. B. (1984). "The fine structure of the lateral superior olivary nucleus of the cat." J Comp Neurol **227**(1): 63-77.

Cant, N. B. and J. H. Casseday (1986). "Projections from the anteroventral cochlear nucleus to the lateral and medial superior olivary nuclei." J Comp Neurol **247**: 457-476.

Cavazzini, M., T. Bliss and N. Emptage (2005). "Ca2+ and synaptic plasticity." Cell Calcium **38**(3-4): 355-367.

Cline, H. and M. Constantine-Paton (1990). "NMDA receptor agonist and antagonists alter retinal ganglion cell arbor structure in the developing frog retinotectal projection." J. Neurosci. **10**(4): 1197-1216.

Cline, H. T., E. A. Debski and M. Constantine-Paton (1987). "N-methyl-D-aspartate Receptor Antagonist Desegregates Eye-Specific Stripes." PNAS **84**(12): 4342-4345.

Colonnese, M. T., J.-P. Zhao and M. Constantine-Paton (2005). "NMDA Receptor Currents Suppress Synapse Formation on Sprouting Axons In Vivo." J. Neurosci. **25**(5): 1291-1303.

Denk, W., J. H. Strickler and W. W. Webb (1990). "Two-Photon Laser Scanning Fluorescence Microscopy." Science **248**(4951): 73-76.

Diaspro, A. and C. Sheppard (2002). Two-photon excitation fluorescence microscopy. Confocal and Two-Photon Microscopy: Foundations, Applications, and Advances. A. Diaspro. New York, Wiley-Liss, Inc**:** 3.3-3.4.

Ehrlich, I., S. Lohrke and E. Friauf (1999). "Shift from depolarizing to hyperpolarizing glycine action in rat auditory neurones is due to age-dependent Cl- regulation." J Physiol (Lond) **520**(1): 121-137.

Ene, F. A., A. Kalmbach and K. Kandler (2007). "Metabotropic Glutamate Receptors in the Lateral Superior Olive Activate TRP-Like Channels: Age- and Experience-Dependent Regulation." J Neurophysiol **97**(5): 3365-3375.

Ene, F. A., P. H. M. Kullmann, D. C. Gillespie and K. Kandler (2003). "Glutamatergic Calcium Responses in the Developing Lateral Superior Olive: Receptor Types and Their Specific Activation by Synaptic Activity Patterns." J Neurophysiol **90**(4): 2581-2591.

Fox, K., B. L. Schlaggar, S. Glazewski and D. D. M. O'Leary (1996). "Glutamate receptor blockade at cortical synapses disrupts development of thalamocortical and columnar organization in somatosensory cortex." PNAS **93**(11): 5584-5589.

Friauf, E., B. Hammerschmidt and J. Kirsch (1997). "Development of adult-type inhibitory glycine receptors in the central auditory system of rats." The Journal of Comparative Neurology **385**(1): 117-134.

Gaiarsa, J.-L., O. Caillard and Y. Ben-Ari (2002). "Long-term plasticity at GABAergic and glycinergic synapses: mechanisms and functional significance." Trends in Neurosciences **25**(11): 564-570.

Gillespie, D. C., G. Kim and K. Kandler (2005). "Inhibitory synapses in the developing auditory system are glutamatergic." Nature Neuroscience **8**(3): 332-338.

Goldberg, J. H., G. Tamas, D. Aronov and R. Yuste (2003). "Calcium Microdomains in Aspiny Dendrites." Neuron **40**(4): 807-821.

Göppert-Mayer, M. (1931). "Über Elementarakte mit zwei Quantensprüngen." Annalen der Physik **401**(3): 273-294.

Gras, C., J. Vinatier, B. Amilhon, A. Guerci, C. Christov, P. Ravassard, B. Giros and S. El Mestikawy (2005). "Developmentally regulated expression of VGLUT3 during early post-natal life." Neuropharmacology **49**(6): 901-911.

Grunze, H. C., D. G. Rainnie, M. E. Hasselmo, E. Barkai, E. F. Hearn, R. W. McCarley and R. W. Greene (1996). "NMDA-dependent modulation of CA1 local circuit inhibition." J. Neurosci. **16**(6): 2034-2043.

Helfert, R. H., J. M. Juiz, S. C. Bledsoe Jr, J. M. Bonneau, R. J. Wenthold and R. A. Altschuler (1992). "Patterns of glutamate, glycine, and GABA immunolabeling in four synaptic terminal classes in the lateral superior olive of the guinea pig." The Journal of Comparative Neurology **323**(3): 305-325.

Hyson, R. L., A. D. Reyes and E. W. Rubel (1995). "A depolarizing inhibitory response to GABA in brainstem auditory neurons of the chick." Brain Research **677**(1): 117-126.

Iwasato, T., A. Datwani, A. M. Wolf, H. Nishiyama, Y. Taguchi, S. Tonegawa, T. Knopfel, R. S. Erzurumlu and S. Itohara (2000). "Cortex-restricted disruption of NMDAR1 impairs neuronal patterns in the barrel cortex." **406**(6797): 726-731.

Joshi, I. and L.-Y. Wang (2002). "Developmental profiles of glutamate receptors and synaptic transmission at a single synapse in the mouse auditory brainstem." J Physiol (Lond) **540**(3): 861-873.

Kandler, K. and E. Friauf (1995). "Development of electrical membrane properties and discharge characteristics of superior olivary complex neurons in fetal and postnatal rats." European Journal of Neuroscience **7**: 1773-1790.

Kandler, K. and E. Friauf (1995). "Development of glycinergic and glutamatergic synaptic transmission in the auditory brainstem of perinatal rats." J. Neurosci. **15**(10): 6890-6904.

Kapfer, C., A. Seidl, H. Schweizer and B. Grothe (2002). "Experience-dependent refinement of inhibitory inputs to auditory coincidence-detector neurons." Nature Neuroscience **5**(3): 247-253.

Katz, L. C. and C. J. Shatz (1996). "Synaptic Activity and the Construction of Cortical Circuits." Science **274**(5290): 1133-1138.

Kim, G. and K. Kandler (2003). "Elimination and strengthening of glycinergic/GABAergic connections during tonotopic map formation." Nature Neuroscience **6**(3): 282-290.

Kotak, V. C., S. Korada, I. R. Schwartz and D. H. Sanes (1998). "A Developmental Shift from GABAergic to Glycinergic Transmission in the Central Auditory System." J. Neurosci. **18**(12): 4646-4655.

Kotak, V. C. and D. H. Sanes (2000). "Long-Lasting Inhibitory Synaptic Depression is Age- and Calcium-Dependent." J. Neurosci. **20**(15): 5820-5826.

Kullmann, P. H. M., F. A. Ene and K. Kandler (2002). "Glycinergic and GABAergic calcium responses in the developing lateral superior olive." European Journal of Neuroscience **15**(7): 1093-1104.

Kullmann, P. H. M. and K. Kandler (2001). "Glycinergic/GABAergic synapses in the lateral superior olive are excitatory in neonatal C57Bl/6J mice." Developmental Brain Research **131**(1-2): 143-147.

Kullmann, P. H. M. and K. Kandler (2008). "Dendritic Ca2+ responses in neonatal lateral superior olive neurons elicited by glycinergic/GABAergic synapses and action potentials." Neuroscience **154**(1): 338-345.

Lee, L.-J., F.-S. Lo and R. S. Erzurumlu (2005). "NMDA Receptor-Dependent Regulation of Axonal and Dendritic Branching." J. Neurosci. **25**(9): 2304-2311.

Lu, T. and L. O. Trussell (2001). "Mixed excitatory and inhibitory GABA-mediated transmission in chick cochlear nucleus." The Journal of Physiology **535**(1): 125-131.

Malenka, R. C. and M. F. Bear (2004). "LTP and LTD: An Embarrassment of Riches." Neuron **44**(1): 5-21.

Marsden, K. C., J. B. Beattie, J. Friedenthal and R. C. Carroll (2007). "NMDA Receptor Activation Potentiates Inhibitory Transmission through GABA Receptor-Associated Protein-Dependent Exocytosis of GABAA Receptors." J. Neurosci. **27**(52): 14326-14337.

McLaughlin, T. and D. D. M. O'Leary (2005). "Molecular Gradients and Development of Retinotopic Maps." Annual Review of Neuroscience **28**(1): 327-355.

McLean, H., O. Caillard, Y. Ben-Ari and J.-L. Gaiarsa (1996). "Bidirectional plasticity expressed by GABAergic synapses in the neonatal rat hippocampus." J Physiol (Lond) **496**(2): 471-7.

Morishita, W. and B. R. Sastry (1996). "Postsynaptic mechanisms underlying long-term depression of GABAergic transmission in neurons of the deep cerebellar nuclei." J Neurophysiol **76**(1): 59-68.

Nabekura, J., S. Katsurabayashi, Y. Kakazu, S. Shibata, A. Matsubara, S. Jinno, Y. Mizoguchi, A. Sasaki and H. Ishibashi (2004). "Developmental switch from GABA to glycine release in single central synaptic terminals." **7**(1): 17-23.

Nevian, T. and B. Sakmann (2006). "Spine Ca2+ Signaling in Spike-Timing-Dependent Plasticity." J. Neurosci. **26**(43): 11001-11013.

Nikolenko, V., B. Nemet and R. Yuste (2003). "A two-photon and second-harmonic microscope." Methods **30**(1): 3-15.

Nimchinsky, E. A., B. L. Sabatini and K. Svoboda (2002). "Structure and Function of Dendritic Spines." Annual Review of Physiology **64**(1): 313-353.

Nishimaki, T., I.-S. Jang, H. Ishibashi, J. Yamaguchi and J. Nabekura (2007). "Reduction of metabotropic glutamate receptor-mediated heterosynaptic inhibition of developing MNTB-LSO inhibitory synapses." European Journal of Neuroscience **26**(2): 323-330.

Nugent, F., E. Penick and J. A. Kauer (2007). "Opiods block long-term potentiation of inhibitory synapses." Nature **446**: 1086-1090.

Nugent, F. S. and J. A. Kauer (2008). "LTP of GABAergic synapses in the ventral tegmental area and beyond." J Physiol **586**(6): 1487-1493.

Ouardouz, M. and B. R. Sastry (2000). "Mechanisms Underlying LTP of Inhibitory Synaptic Transmission in the Deep Cerebellar Nuclei." J Neurophysiol **84**(3): 1414-1421.

Ruthazer, E. and H. Cline (2004). "Insights into activity-dependent map formation from the retinotectal system: A middle-of-the-brain perspective." Journal of Neurobiology **59**(1): 134-146.

Sanes, D. (1993). "The development of synaptic function and integration in the central auditory system." J. Neurosci. **13**(6): 2627-2637.

Soler-Llavina, G. J. and B. L. Sabatini (2006). "Synapse-specific plasticity and compartmentalized signaling in cerebellar stellate cells." Nature Neuroscience **9**(6): 798-806.

Staley, K. J. and I. Mody (1992). "Shunting of excitatory input to dentate gyrus granule cells by a depolarizing GABAA receptor-mediated postsynaptic conductance." J Neurophysiol **68**(1): 197-212.

Stelzer, A., N. Slater and G. ten Bruggencate (1987). "Activation of NMDA receptors blocks GABAergic inhibition in an in vitro model of epilepsy." Nature **326**: 698-701.

Tyszkiewicz, J. P., Z. Gu, X. Wang, X. Cai and Z. Yan (2004). "Group II metabotropic glutamate receptors enhance NMDA receptor currents via a protein kinase C-dependent mechanism in pyramidal neurones of rat prefrontal cortex." J Physiol **554**(3): 765-777.

Wang, J. H. and A. Stelzer (1996). "Shared calcium signaling pathways in the induction of long-term potentiation and synaptic disinhibition in CA1 pyramidal cell dendrites." J Neurophysiol **75**(4): 1687-1702.

Wise, F. (1999). Lasers for two-photon microscopy. Imaging: A Laboratory Manual. R. Yuste, F. Lanni and A. Konnerth. Cold Spring Harbor, NY, Cold Spring Harbor Press**:** 18.1-18.9.

Yasuda, R., E. A. Nimchinsky, V. Scheuss, T. A. Pologruto, T. G. Oertner, B. L. Sabatini and K. Svoboda (2004). "Imaging Calcium Concentration Dynamics in Small Neuronal Compartments." Science's STKE **2004**(219): pl5-.

Yuste, R., A. Majewska and K. Holthoff (2000). "From form to function: calcium compartmentalization in dendritic spines." **3**(7): 653-659.